AN EXPERIMENTAL INVESTIGATION OF SOUND TRANSMISSION THROUGH A FLEXIBLE PANEL INTO A CLOSED CAVITY

by

George F. Gorman, III

AMS Report No. 925

July 1970

NGR-31-001-146

ACKNOWLEDGEMENTS

It is with pleasure that I acknowledge the assistance and guidance given me by my advisor, Professor Earl H. Dowell. I would also like to thank the National Aeronautics and Space Administration for allowing me to further my education through the use of a NASA Traineeship, and for supporting this research in part by NASA Grant NGR 31-001-146.

This thesis carries No. 925-T in the records of the Department of Aerospace and Mechanical Sciences.

TABLE OF CONTENTS

LIST OF FIGURES

NOMENCLATURE

a - panel length

a_c - speed of sound

a^{d_i} - panel deflection @ depth d_i

a_{mn} - A_{mn} / h

A_{mn} - modal amplitude

b - panel width

b_{ij} - modal amplitude

B_{ij} - transformed b_{ij}

c - coefficient of viscous damping

d - cavity depth

d_i - incremental cavity depth

d_o - pickup separation

D - panel stiffness

f - frequency (rad./sec.)

h - panel thickness

k - spring coefficient

K_{mn} - non-dimensional frequency

K_{mn}^{∞} - non-dimensional frequency @ d = ∞

m - panel mass

n_c - critical damping coefficient

$p_c - p_{\infty}^c$ - fluid pressure, cavity flow

p^{d_i} - cavity pressure @ depth d_i

$P_c - P_{\infty}^c$ - transformed $p_c - p_{\infty}^c$

$\tilde{p}$ - pd/a_c

$\Delta P_{external}$ - external pressure loading

q_n - non-dimensional panel deflection

Q_{mrns}^c - generalized aerodynamic force

$Q_{rs}^{external}$ - generalized external force

s_c - ta_c/a

t - time

w - panel deflection

x, y, z - spatial coordinates

$\ddot{X}_m$ - amplitude of m^{th} pulse

β - damping

δ - panel deflection

∇ - differential operator

ζ^{d_i} - damping ratio @ d_i

ζ_n - damping ratio of n^{th} mode

ζ - z/d

η - y/b

λ_c^* - $\rho_c a_c^2 a^3/D$

λ_c - $\rho a_c^2 a^3/D$

ν - Poisson's ratio

ξ - x/a

ρ - air density

ρ_c - cavity density

σ_c - dummy S_c

ϕ_c - velocity potential

ϕ^c_{ij} - modal amplitude

Φ^c_{ij} - transformed ϕ^c_{ij}

ψ_m, ψ_n - modal functions

ω_n - frequency of n^{th} mode

Ω^{d_i} - frequency @ depth d_i

I. INTRODUCTION

1.1 Reason for Interest

The subject of sound transmission through a flexible wall has received much attention in the past few years. In particular, much of this interest has centered around the effect of a cavity on the vibrations of a panel. This investigation is concerned with a somewhat simplified geometry, that of a rigid rectangular cavity with one flexible wall, and with a somewhat simplified exciting force, that of a sinusoidal acoustic driving force. See Figure 1.

One reason for the interest in this problem is its application to various other problems of a more practical nature. Two main problems that exist are the response of aircraft skin panels to boundary layer turbulence, and the response of rooms to vibrations of the walls. Wings (and fuselages) are constructed in such a way that there exists a shallow cavity between the upper and lower surfaces of the wing. Although the wing problem is very complex due to the irregular cavity shape and due to the random flow over both surfaces of the wing, a consideration of the simplified problem being discussed here will give some insight into the more complex problem of wing response. Likewise, the response of rooms to vibrations of the walls is also a complex problem, even if the room is rectangular. Aside from the obvious complexity of having all the walls of approximately the same stiffness and therefore all

deflecting similarity under the influence of an acoustic driving force, one must confront the problem of windows and doors, and also the location of other rooms with respect to the room being analyzed. However, again, the simplified problem that is considered here will give some insight into the more complex problem of room response.

1.2 Analytical Techniques

Although the wing problem and the room problem seem similar, the usual method for the theoretical analysis of each of these problems is very different. Morse and Ingard[1] have shown that for cavities that are smaller than, or of the same size as, a wavelength of the exciting force, the analysis is done in terms of the normal modes of the system. This is the case in the wing problem, where frequency components whose wavelengths are on the order of the size of the airfoil thickness are often encountered. Inherent in an analysis of this problem is a concern for the coupled nature of the system: the panel is first excited by some sort of pressure wave; the resulting motion of the panel produces an acoustic, or pressure oriented, disturbance in the cavity which in turn creates a back pressure that effects the motion of the panel. However, for cavities that are much larger than a wavelength, as in the room problem, it might be more convenient to use geometrical acoustics and follow the "rays" of sound as they bounce back and forth in the cavity.

There is one case, however, that has recently generated much concern in which one uses the modal techniques to solve for the

response of rooms. This special case is the response of rooms to a sonic boom, or "N-wave" excitation. Studies by NASA[2,3] have indicated that the period of such an N-wave is on the order of 0.1 second. Thus, the wavelength of such a pulse is on the order of 100 ft., which is well above most room dimensions. Since, in the present analysis, we will be dealing with frequencies whose wavelengths are on the order of the cavity size, given the proper external pressure field, one could predict the response of rooms to a sonic boom type excitation. Therefore, although the model being considered is very simplified compared to most of the real problems that exist, this model could be used as a starting point for these more complex problems.

Numerous authors have examined the problem of sound transmission using one of the methods outlined previously to obtain theoretical results. Experimental results, however, are sadly lacking. Aside from Dowell and Voss[4] wind tunnel experiments concerning the flutter of flat plates, and acoustical experiments by Pretlove and Craggs[5], there has been little experimental data to verify existing theory. Furthermore, most of the experimental data that were obtained were frequency oriented, i.e., dealing with cavity effects on panel natural frequencies, with very little work done concerning panel amplitudes or cavity pressures as a function of cavity depth. It is one of the purposes of the present experimental work to present a fuller range of data than has been obtained previously.

1.3 Cavity-Panel Interaction Effects

Before discussing the experimental program, it will be beneficial to outline some of the main effects that have been noted in previous work of the type under discussion here. First, at shallow cavity depths, the coupling between panel modes becomes unimportant.[4] When this coupling does occur, significant changes from the panel "in-vacuo" mode shapes may be produced. For example, the coupling between the first and third panel modes is significant. See Figure 2. As the cavity depth decreases ($a/d \to \infty$), the panel fundamental mode forms two modal lines and takes on many of the characteristics of the third panel mode. The effect on the third panel mode is similar. As the cavity depth decreases ($a/d \to \infty$), the third panel mode loses its two nodal lines, and takes on some of the characteristics of the panel fundamental mode. The coupling between higher panel modes is similar to the coupling between the first and third panel modes.

Also noted previously were the effects of cavity depth on panel natural frequencies. For the panel fundamental mode and the higher symmetric modes, the effect of decreasing cavity depth is increasing panel natural frequencies, the so-called "stiffness effect". This effect is not present in the antisymmetric modes. In the antisymmetric modes, just the contrary is true: the effect of decreasing cavity depth is decreasing panel natural frequencies, the so-called "virtual mass effect". These two effects have been studied and can be explained fairly easily.[6,7,8]

The virtual mass effect is due to the air within the cavity

acting as an additional mass on the panel. This additional mass causes a decrease in the natural frequencies of all of the panel modes, not just the antisymmetric modes, as the cavity depth is decreased. However, this additional mass is small compared to the panel mass, and thus the effect is small.

The stiffness effect is due mainly to the compressibility of the air within the cavity. In the case of the panel fundamental mode, or any symmetric panel mode, as the panel oscillates, it forces the air in the cavity downward and, in effect, produces a volume change in the cavity. See Figure 3. The air in the cavity due to its compressibility, acts as an aerodynamic spring and thus stiffens the panel. Since the panel frequencies are directly related to the stiffness, this increased stiffness causes an increase in the frequencies of the symmetric panel modes.

For the antisymmetric panel modes, there is no net volume change as the panel oscillates. See Figure 4. Therefore, the stiffness effect is not present for the antisymmetric panel modes, and thus the only effect present for these modes is the virtual mass effect, even though it is small. Since the influence of the virtual mass effect is small, the stiffness effect is the main effect acting on the symmetric panel modes, even though the virtual mass effect is present.

Thus, in review, there are two main cavity effects acting on the panel: the stiffness effect and the virtual mass effect. The virtual mass effect is present in all panel natural modes and is due to the mass of the air within the cavity; whereas, the stiffness

effect is present only in the symmetric panel modes and is due to the compressibility of the air within the cavity. Both of these effects vary the natural frequencies of the panel and cause intermodal coupling at shallow cavity depths.[4,5]

The final effect to be considered is the effect of frequency and cavity depth on the damping ratio of both the panel and the cavity. The interaction effects on panel and cavity damping ratios have not been investigated previously, however, some insight may be gained by considering the panel and cavity separately. Theoretically, for damping that is proportional to panel velocity, the damping ratio of the panel varies as the inverse of the frequency.[9]

To see this result more clearly, consider a one dimensional plate with velocity damping:

$$D\frac{\partial^4 w}{\partial x^4} + \beta\frac{\partial w}{\partial t} + m\frac{\partial^2 w}{\partial t^2} = 0$$

and assume

$$w = q_n(t)\sin\frac{n\pi x}{a}$$

then one obtains

$$\omega_n^2 q_n + 2\zeta_n\omega_n\frac{dq_n}{dt} + \frac{d^2q_n}{dt^2} = 0$$

where

$$\omega_n \equiv (n\pi)^2\left[D/ma^4\right]^{1/2}$$

and

$$\zeta_n \equiv \beta / 2 m \omega_n .$$

Since β is assumed constant, then, by taking the ratio of the damping ratio of the n^{th} natural frequency to the fundamental frequency one obtains:

$$\frac{\zeta_n}{\zeta_1} = \frac{\omega_1}{\omega_n} .$$

Thus, the damping ratio varies as the inverse of the frequency for a panel with velocity damping. Other types of damping are discussed by Dugundji.[9]

There has been very little work done in the area of cavity damping. Most analyses have been concerned with cavity damping in the time domain, whereas the main consideration in this report is cavity damping in the frequency domain. Sheshadri[10] has presented a fairly concise evaluation of the damping of Helmholtz resonators. His analysis discusses damping due to the low frequency movement of air in the neck of the resenator. By considering the damping due to viscous losses, radiation losses, heat conduction losses, and other losses such as mechanical wall vibrations and gaseous absorbtion due to thermal relaxation, the net damping ratio was computed to be

$$\zeta = \frac{fA}{2a_c L} + \frac{1}{2}\left(\frac{\nu}{Af}\right)^{1/2} + 0.265\left(\frac{\nu}{Af}\right)^{1/2}$$

where A is the area of the neck and L is the length of the neck.

Since the present analysis is concerned mainly with relatively high frequency damping, the usefulness of Sheshadri's equation is questionable. However, Sheshadri's analysis does form a basis to which the damping results in this report can be compared. For additional panel and cavity calculations, the reader is referred to References 11, 12, 13 and 14.

II. EXPERIMENTAL PROGRAM

2.1 Experimental Arrangement

As with any experimental program, this research had as its goals the verification of existing theory and experiment, and the possible formulation of a new, perhaps more complete, theory. The experimental arrangement used to accomplish these goals is shown in Figure 5.

The panel was a 10" x 20" x 0.05" aluminum alloy plate that was bonded onto a rectangular frame consisting of aluminum channel members welded together at their ends. By bonding the plate to the cavity in this way, a clamped edge boundary condition was approximated. A sealed cavity was constructed beneath the panel in such a way that the cavity depth could be varied in 2 inch increments from 12" to 2" deep. In order to vary the cavity depth, the cavity was built in sections. Each 2 inch section of the cavity was bolted to the other sections with rubber gaskets between them. The cavity itself was made of 0.5" thick plexiglass and was supported by four plexiglass "feet".

The panel was excited acoustically by a Wolverine LS15, 20 watt loudspeaker driven by a B & K Beat Frequency Oscillator, type 1022. The external sound field was set at 100 dB on the plate surface for all measurements.

The use of a single speaker for panel excitation did present some problems, particularly in coordinating theoretical work with this

experiment. The ideal external sound field would have a constant amplitude in space over the whole surface of the panel. By using a single speaker, an external field distribution that was not constant in space was obtained, but rather its amplitude was approximately 9 dB lower at the point of maximum panel length, and about 2 dB lower at the point of maximum panel width than at the panel center. See Figure 6. Although this distribution is not ideal, it can be approximated in a computer simulation to obtain comparisons between theory and experiment.[15]

The panel-cavity system was placed on a laboratory bench inside a specially designed acoustic chamber. This acoustic chamber was designed to reduce the sound transmission from the laboratory to the experiment, to reduce the sound transmission from the loudspeaker into the laboratory, and thus, to isolate the experiment as much as possible from extraneous noise.

The acoustic chamber was constructed of 1/2" plywood on a frame made of 2" x 4" beams and was 7'8" x 8'0" x 7'6". The interior wall of the chamber was lined with 24" x 48" x 1/2" acoustical tiles on all four walls and on the ceiling. A nylon carpet with backing was used on the floor of the chamber. Between the exterior plywood walls and the interior acoustic tile walls, fiberglass insulation was used to reduce the sound transmission further. The room was placed on 1" thick felt blocks in order to reduce the structural vibrations of the laboratory from exciting the acoustic chamber. A 1 3/4" thick solid wood door was used in one wall and was lined with acoustic tile on its inside face. A 10" x 12" x 1/4"

double window made of plexiglass was used in the door to enable observation from outside of the chamber. The use of a double window reduces sound transmission through the window. See Figure 7.

Since the acoustic chamber itself is a cavity, it has its own natural frequencies and normal modes. The fundamental frequency of the chamber was measured experimentally to determine if chamber acoustics would interfere with the experiment. The fundamental frequency of the chamber was found to be 70 cps, which is below the frequency range to be investigated (100 cps to 2000 cps). The room resonances at the higher frequencies were of a sufficiently low amplitude as to be of no significance. Therefore, chamber acoustics were neglected in all measurements.

Initially, there were two basic measurements that were felt to be important: the measurement of panel amplitude and the measurement of cavity pressures due to a sinusoidal driving force. As work progressed, however, the need arose for two more measurements: the measurement of panel and cavity damping ratios. The reasons for these latter measurements will become apparent later.

2.2 Panel Amplitude Measurement

The panel motion was measured by the use of a Bently Nevada motion pickup, Model 302, that was mounted on an aluminum frame located above the panel. The frame allowed movement of the pickup to any point on the surface of the panel, and also allowed variation of the distance between the pickup and the panel. Since the output of the pickup depends on the distance from the pickup to the panel,

this distance must be chosen carefully so as to stay within the linear range of the pickup, and must remain constant throughout the testing procedure. To insure that the static gap distance did remain constant throughout the testing procedure, an oscilloscope was used to measure this distance in volts and to set the static gap before each run. As the panel oscillated, the voltage generated by the motion pickup was fed through an amplifier and recorded on a amplitude vs. frequency plot. Such a plot is shown in Figure 8, for a cavity depth of 12".

For the measurement depicted in Figure 8, the motion pickup was positioned at the center of the panel. By positioning the pickup in this way, one may obtain deflection measurements for the symmetric panel modes, i.e., the modes which have a peak at the panel center, but not for the antisymmetric modes, i.e., those modes with a node at the panel center. Notice that the dominant features of the plot are the three resonant peaks, corresponding to the first, third and fifth panel modes, occuring at 113 cps, 210 cps and 410 cps. Modes above the fifth mode have an amplitude that is negligible compared to the first three symmetric modes. Notice that, above 500 cps, the panel is essentially motionless. Also notice that, by far, the dominant panel response is at the panel fundamental mode, as is expected.

2.3 Cavity Pressure Measurement

The pressure, or sound level, within the cavity, when the panel has been excited by the loudspeaker, was measured using a B & K 1/4"

microphone, Type 4136 with a Type 2615 cathode follower with Type UA 0035 connector. This microphone was installed in holes that were drilled in the side of the cavity and that were plugged up when not in use so as to insure a near leak-proof cavity. These holes were spaced at cavity depths of 3", 5", 7", 9" and 11", so that the pressure variation with cavity depth could be studied. As with the panel motion pickup, the voltage from the microphone due to excitation of the cavity was recorded on a amplitude vs. frequency plot. Such a plot is shown in Figure 9, for a cavity depth of 12".

For the measurement depicted in Figure 9, the microphone was positioned in the hole located at the 3" cavity depth level. Since all theoretical calculations involve the cavity pressure at a point just beneath the panel, the 3" depth level was chosen to place the microphone as close to the undersurface of the panel as possible. Notice that in Figure 9, the cavity pressure was plotted against frequency, where this pressure is the difference between the dB level inside the cavity and the dB level outside the cavity on the upper surface of the panel. Again, the dominant features are the three primary resonant peaks occuring at 113 cps, 210 cps and 518 cps. The first two resonances correspond to the first and third panel modes, and thus indicate that the panel is driving the cavity at these frequencies. The resonance at 518 cps is the fundamental cavity mode. Notice that this mode occurs above the frequency at which the panel becomes motionless (500 cps), and thus, in effect, the cavity is acting as a rigid cavity with no flexible

walls. Theoretically, since the panel is motionless, the pressure level difference between the external and internal measurements should be zero. Notice that this is practically the case in Figure 9, the slight variation from zero due to the very slight motion of the panel at this frequency. Notice also that, as with the panel amplitude, the greatest cavity response occurs at the panel fundamental frequency, with the second greatest response occurring at the cavity fundamental frequency.

2.4 Damping Ratio Measurement

The damping ratios of the panel and cavity can be measured experimentally in two different ways: the first, by using an oscilloscope and what is termed the "peak method", and the second, by using an oscillograph and what is termed the "decay method".[16]

The peak method determines the damping ratio from a plot of amplitude vs. frequency at a resonance. See Figure 10a. It can be shown that for small damping, at a point where the amplitude is $1\sqrt{2}$ times the resonant amplitude, that $\Delta\omega = \delta\omega_o\pi$ where δ is the logarithmic decrement ($= \log x_1/x_2$), and where ω_o is the resonant frequency. If we consider a simple spring-mass-damper system, the equation of motion for free vibration is

$$\ddot{x} + c\dot{x} + kx = 0$$

If we define $n \equiv c/2$ and $p^2 \equiv k$, then the equation of motion becomes

$$\ddot{x} + 2n\dot{x} + p^2x = 0.$$

Now, the general solution to this equation is

$$x = c_1 e^{(-n+\sqrt{n^2-p^2})t} + c_2 e^{(-n-\sqrt{n^2-p^2})t}$$

where c_1 and c_2 are constants. The physical significance of this solution depends on the relative magnitudes of n^2 and p^2. When $n^2 = p^2$, the system is critically damped and $n_c \equiv n$. Thus, from Figure 10b, one can show that

$$\frac{x_1}{x_2} = e^{-nt_1} \Big/ e^{-n\left(t_1 + \frac{2\pi}{n_c\sqrt{1-(n/n_c)^2}}\right)}$$

$$= e^{\frac{2\pi n}{n_c\sqrt{1-(n/n_c)^2}}}$$

Now, since $\delta \equiv \log \frac{x_1}{x_2}$, then

$$\delta = 2\pi (n/n_c) \Big/ \sqrt{1-(n/n_c)^2}.$$

If we assume small damping, so that $n << n_c$, then

$$\delta \approx 2\pi \left(\frac{n}{n_c}\right) = 2\pi\zeta$$

However, from before we know that

$$\delta = \pi \Delta\omega / \omega_o$$

thus:

$$\zeta = \frac{\Delta\omega}{2\omega_o}$$

This peak method, although fairly easy to use, is hard to measure for very small damping ratios where there is error in measuring the width of the resonant peak which is very narrow. Therefore, this method was used only to check the second method of measurement, the decay method, and not to obtain precise numerical results.

The decay method determines the damping ratio from a plot of amplitude versus time. See Figure 10b. If the amplitude of the initial pulse is x_1 and the amplitude of the m^{th} pulse is x_m, then, setting $t_1 \equiv 0$:

$$\frac{x_1}{x_m} = 1 \Big/ \left[e^{-n 2\pi\omega_o t_m / n_c \sqrt{1-(n/n_c)^2}} \right]$$

or

$$\frac{x_1}{x_m} = e^{\left[2\pi \zeta \omega_o t_m / \sqrt{1-\zeta^2}\right]}$$

and thus:

$$\zeta = \frac{1}{2\pi\omega_o t_m} \ln\left(\frac{x_1}{x_m}\right)$$

As mentioned previously, the decay method was the method used to experimentally determine damping ratios. The actual measurement of damping ratios was as follows: using an oscillograph, a plot of amplitude vs. time was obtained. As the oscillograph was recording,

the voltage to the loudspeaker was cut off, thus eliminating the external sound field, and the classic exponential decay plot was obtained. Then, the decay method formula was used to compute damping ratios.

Figure 11, plots the damping ratio of the panel with a 12" deep cavity as a function of frequency. The experimental points were measured at the first, third and fifth panel modes for this panel - cavity configuration. The curve obtained is consistent with a theoretical model, which says that for damping that is proportional to panel velocity, the damping ratio varies as the inverse of the frequency.[9] The slight variation from theory at the higher panel frequencies is probably due to coupling between the panel and cavity modes.

Figure 12, plots the damping ratio of the cavity (12" depth) as a function of frequency. The experimental points were measured at the first, second and third cavity depth modes. The curve obtained suggests that the cavity damping ratio at a constant cavity depth varies as the inverse of the frequency squared. This result is inconsistent with Sheshadri,[10] concerning the damping of Helmholtz resonators, and also does not agree with the variation of panel damping with frequency at a constant cavity depth. As yet, no explanation can be given for this damping result, other than to conclude that such a result seems to indicate a more complex damping mechanism than that of the panel. For the panel, the damping was assumed to be proportional to the velocity of the panel. For the cavity, such a simple relationship cannot be assumed.

III. EXPERIMENTAL RESULTS

Having reviewed the results of previous research, and having discussed the experimental apparatus, one may now proceed to the results of the present work. The present research, for the most part, deals with measurements of panel amplitudes and cavity pressures, along with measurements of some of the panel-cavity interation mechanisms discussed previously. In addition, some measurements of panel and cavity damping ratios have been included to supplement and help explain the panel amplitude and cavity pressure measurements.

3.1 Panel Frequency Response

Since the panel-cavity system being discussed is an integrated system, one must investigate the coupling effects between the panel and cavity. Previous work seems to indicate that the cavity effect on the panel will become more pronounced as the cavity depth decreases.[6] This fact is apparent in Figures 13 and 14. In Figure 13, the panel deflection, normalized about the mid-point of the panel, has been plotted against the panel length, normalized with the total panel length, for the fundamental mode of the panel backed up by a 12" and a 2" deep cavity. Figure 14, plots a similar response, only normalized about the one-third point of the panel, for the third panel mode. These graphs depict the effect of intermodal coupling at shallow cavity depths. The panel response at the 12" depth for both the first and third panel modes

is very close to the "in-vacuo" curve given by Dowell and Voss,[4] indicating that, for the panel size investigated here, a 12" deep cavity approximates an infinite cavity fairly effectively.

For a cavity depth of 2", the mode shapes vary considerably. In the case of the panel fundamental mode, the response is more concentrated about the center of the panel than for the 12" depth case. The response can be seen to be approaching the shape of the third mode, indicated intermodal coupling at this shallow cavity depth. Indeed, if the cavity was made more shallow, the panel fundamental mode would take on the modal pattern of the third mode by having two nodal points.[4,6] For the third panel mode at the 2" cavity depth, the change in modal shape is less dramatic. However, there is some effect, especially around the mid-point of the panel, and this measured effect corresponds to the results of Dowell and Voss. Again, is the cavity were made more shallow, the effect would be more dramatic with the probable elimination of all nodal points,[4,6] indicating intermodal coupling between the first and third panel modes.

Aside from affecting the mode shapes of the panel, the cavity also affects the natural frequencies of the panel due to the stiffness and virtual mass effects discussed previously. In Figure 15, the panel fundamental frequency is plotted against cavity depth. Note that, as the cavity depth decreases, the panel fundamental frequency increases from 112.8 cps to 137.0 cps. This increase in frequency is an excellent example of the stiffness effect, for, as

the cavity depth is decreased, the cavity becomes stiffer, thus raising the panel natural frequency. Figure 16, plots the panel frequencies vs. cavity depth for the third and fifth panel modes. Note that there is apparent a slight stiffness effect on the third mode, and the lack of any stiffness effect on the fifth mode. In fact, the fifth panel mode displays features of the virtual mass effect, for as the cavity depth decreases, the natural frequencies decrease also. This fact also indicates that the virtual mass effect is present in symmetric panel modes, and not just in the antisymmetric modes. The frequency response for the third and fifth panel modes is consistent with theory, which states that the stiffness effect becomes less for the higher symmetric modes and that the virtual mass effect is present in all modes.[4]

In order to compare theory and experiment, a twofold method of computation must be used. First, the panel natural frequencies must be computed for the infinite cavity, or "in-vacuo", case. Second, these computed values of the panel frequencies must be modified to consider the effects of a cavity on the panel.

The method chosen to compute the panel "in-vacuo" frequencies was discussed by Warburton.[17] Starting from the plate equation

$$D\nabla^4 w + m\frac{\partial^2 w}{\partial t^2} = 0$$

and using a Rayleigh-Ritz method, assuming that the waveforms of plates and beams are similar (i.e., for all edges clamped, the

waveform is assumed to be the product of the characteristic functions of two beams with fixed ends), Warburton obtains an approximate formula expressing the plate frequency in terms of the boundary conditions, the modal pattern, the plate dimensions, and the constants for the material. Although this method is essentially a one mode approximation, and therefore, less accurate than some of the more exotic methods, it lends itself well to the computation of panel modes in our case, including the higher panel modes. For a panel clamped at all four edges, the natural frequencies may be computed by:

$$K_{mn}^2 = G_m^4 + G_n^4 (a/b)^4 + 2 H_m H_n (a/b)^2$$

where K_{mn} are the non-dimensional panel frequencies, and

$$G_1 = 1.506\pi$$

$$H_1 = 1.248\pi^2$$

$$G_m = \left[\frac{2m+1}{2}\right]\pi \qquad m \geq 2$$

$$H_m = G_m^2\left(1 - \frac{2}{G_m}\right) \qquad m \geq 2 .$$

Dowell and Voss[4] have originated a method for computing the effect of a cavity on the vibrations of a panel. Using the acoustic wave equation and the boundary condition that there is no movement of the cavity walls except for the panel, and assuming a cosine series expansion for the panel deflection, the velocity potential is computed. Then, using the plate equation, expanding the panel deflection in terms of the characteristic functions for a clamped plate, and using Bernoulli's equation for the back pressure on the panel, an equation is obtained for the panel natural frequncies by using Galerkin's method. Given is a one term solution for the fundamental panel frequency, and a two term solution for both the fundamental and third panel frequencies.

One term solution:

$$K_{11}^2 = K_{11_{\text{in vacuo}}}^2 + \frac{4}{9}\lambda_c \frac{a}{d}$$

Two term solution:

$$\begin{vmatrix} A - \frac{9}{4}K^2 + \lambda_c \frac{a}{d} & -B + \frac{3}{4}K^2 \\ -B + \frac{3}{4}K^2 & C - \frac{3}{2}K^2 \end{vmatrix} = 0$$

where

$$A \equiv (2\pi)^4 \left[\frac{3}{4} + \frac{1}{2}(a/b)^2 + \frac{3}{4}(a/b)^4\right]$$

$$B \equiv (2\pi)^4 \left[\frac{3}{4} + \frac{1}{2}(a/b)^2 + \frac{1}{4}(a/b)^4\right]$$

$$C \equiv (2\pi)^4 \left[\frac{3}{4}(17) + \frac{1}{2}(17)(a/b)^2 + \frac{1}{2}(a/b)^4\right]$$

In Figure 17, the ratio of panel frequency to "in-vacuo" panel frequency is plotted against a/d, in order to obtain theoretical points at d = ∞. As mentioned previously, the "in-vacuo" panel frequencies were computed from Warburton's theory,[17] and the panel frequencies' variation with cavity depth were computed from Dowell and Voss' theory.[4] Notice that there is excellent agreement between theory and experiment at the large cavity depths, with some variation from theory occurring at shallow cavity depths. This agreement between theory and experiment seems to indicate that below an a/d of 10, for a panel with similar size, thickness and material properties as the one investigated in this report, a one-term approximation to the panel natural frequencies may be

used to within good accuracy. For a/d > 10, higher term approximations must be employed. In general then, for $\lambda_c a/d > 10{,}000$ (and a/b = 2) higher term approximations must be used to compute panel natural frequencies.

3.2 Cavity Frequency Response

The cavity also responds in certain characteristic modes. Theoretically, at low frequencies below the cavity fundamental, the cavity pressure should be constant with cavity depth since the cavity is responding in its "zeroth" mode. Figure 18, plots the cavity pressure, normalized with the external pressure, versus cavity depth at the panel fundamental frequency. Apparent, is the fact that the cavity pressure distribution is not exactly constant, but displays another waveform. Since the panel fundamental (112.8 cps) is well below the cavity fundamental (518 cps), the response should be constant. This variable response could be due to the nonrigid cavity walls (since the panel is moving greatly), or perhaps some coupling with other cavity modes.

Figure 19, plots a similar normalized pressure distribution at the cavity fundamental depth frequency. Theory predicts that the cavity should respond in a cosine mode, with the internal and external pressures equal at the top and bottom of the cavity, and with the response undergoing a phase shift with cavity depth. Note that the experimental pressure distribution in the cavity at the cavity depth fundamental follows the theoretical cosine curve fairly well except at the deepest part of the cavity. The pressure

reading at this depth is probably due to slight movement of the cavity base. One would expect good agreement with theory at this frequency, since the panel is moving very little, as can be seen in Figure 8.

The pressure distributions at shallow cavity depths were not determined since, at these shallow depths, the size of the microphone became on the order of the cavity depth, and thus true readings could not be obtained. However, at a cavity depth of 4", there was a phase shift at the fundamental cavity depth mode, indicating that perhaps the cosine mode shape predicted by theory is valid at this cavity depth also.

As the cavity depth decreases, there will be an effect on the cavity natural depth frequency. The solution to the wave equation can be given in terms of the speed of sound in the cavity, the physical dimensions of the cavity, and the mode being considered:[1]

$$\omega = \frac{c}{2}\left[\left(\frac{I}{d}\right)^2 + \left(\frac{J}{a}\right)^2 + \left(\frac{K}{b}\right)^2\right]^{1/2}$$

If we consider only the fundamental depth mode (J=K=0), this equation reduces to:

$$\omega = \frac{c}{2}\left(\frac{I}{d}\right)$$

This equation is plotted in Figure 20, along with the experimental points. Note that the experiment agrees quite well with theory,

with the slight variation probably due to a slight variation in cavity depth (due to the rubber gaskets), and perhaps some movement of the panel. However, one may conclude that, for frequencies above the cavity fundamental depth mode, the effect of the panel on the frequencies of the cavity is negligible.

3.3 Panel Displacement and Damping Effects

In Appendix C, the basic theory concerning the coupling of panel and cavity is outlined. From that theory, some basic, one-term approximations for the panel displacement and cavity pressure may be computed. Using such a one-term approximation, one may easily compute the relationship between panel displacements at various cavity depths, in terms of the panel natural frequencies and panel damping ratios:

$$\frac{a^{d_1}}{a^{d_2}} = \left[\frac{\zeta^{d_2}}{\zeta^{d_1}}\right]\left[\frac{\Omega^{d_2}}{\Omega^{d_1}}\right]^2$$

where a is the panel amplitude, ζ is the panel damping ratio, Ω is the panel natural frequency, and the superscripts d_1 and d_2 refer to the various cavity depths. Thus, it is apparent that, aside from panel natural frequencies at the various cavity depths, a knowledge of the panel damping ratios at these various depths is needed. Notice also, however, that, if the panel damping ratio was constant with cavity depth, the ratio of panel amplitudes at

various depths would depend only on the ratio of natural frequencies squared. This however is not the case, for, at the very least, there will be some effect on the panel damping ratios due to the increase of the panel fundamental frequency with cavity depth.

There are three types of damping that will be referred to throughout the rest of this report: constant damping, frequency damping, and experimental damping. Constant damping is the damping ratio obtained if one assumes that there is no variation of panel damping ratio with cavity depth. Frequency damping is the damping discussed previously in which the panel damping ratio was measured at a 12" cavity depth for various panel resonances. Thus, the only effect varying this type of damping is the variation of frequency. And experimental damping is the damping ratio measured experimentally for the exact conditions under investigation. Thus, experimental damping takes into account frequency variations, and depth variations.

Figure 21, plots the panel damping ratio due to the effect of increasing frequency alone, and from experiment. Note that the frequency effect forces the panel damping ratios lower, whereas, the experimental damping ratios are higher, as the cavity depth is reduced. The reasons for this behavior are not readily apparent; however, it is felt that, if there were some leakage from the cavity thus creating more losses in the system, the effect would be to make the panel respond less ideally, i.e., to increase the damping ratio. Preliminary experiments have pointed out that the cavity pressure increases with a decrease in cavity depth. Thus, if there

were a leak present, the effect would be greatest at the shallow cavity depths. This reasoning is consistent with the experimental results depicted in Figure 21.

Figure 22, plots the experimental damping ratio for the third and fifth panel modes, along with the damping ratio due only to the frequency effect. Note that a similar result to that of the fundamental mode is apparent, i.e., the experimental damping ratios are greater than that due to the frequency effect. However, the effect is less apparent for the higher panel modes, indicating that the effect of damping variation on panel modes, is less critical for the higher panel modes than it is for the fundamental panel mode. Since panel damping has been shown to be proportional to the panel velocity (and hence, the $1/\omega$ variation), at the higher panel modes the panel velocity is less than at the fundamental, and thus the effect of damping is less on higher modes.

Now that the panel damping ratios have been determined, the theory outlined in Appendix C, may be used to compute a one-term solution for the panel amplitude, for three cases: constant damping effect, frequency damping effect and experimental damping effect. These results have been plotted in Figure 23, along with the experimental panel amplitudes. Notice that the constant damping and frequency damping cases predict the correct panel amplitudes only at large cavity depths; however, the experimental damping ratios predict the panel amplitudes well throughout the range of cavity depths tested. From this, one may conclude that, given the

proper damping ratios, a one-term approximation for the panel amplitudes is accurate within the range of cavity depths tested. Also, one may conclude that damping, and not frequency, is the critical factor for determining panel amplitudes at various cavity depths.

A similar result may be seen in Figure 24, where panel amplitudes for the third and fifth panel modes are plotted for various cavity depths. Again, the experimental damping ratio predicts the panel amplitudes more accurately than the frequency damping effect. The slight divergence from theory at the shallow cavity depths is probably due to the limitations of one-term theory for the higher panel modes. For these higher modes, a higher-term theory must be used with the correct panel damping ratios to predict panel amplitudes.

3.4 Cavity Pressures and Damping Effects

As with the panel, the theory in Appendix C, may be used to compute cavity pressures. Using a one-term approximation and the theory outlined in the Appendix, the ratio of cavity pressures at various cavity depths can be shown to be:

$$\frac{p^{d_1}}{p^{d_2}} = \frac{d_2}{d_1}\left[\frac{\zeta^{d_2}}{\zeta^{d_1}}\right]\left[\frac{\Omega^{d_2}}{\Omega^{d_1}}\right]^2$$

where d_2 and d_1 are the two cavity depths, and the other factors

are as described previously. Using that previous result, a simplified form of the above equation is found:

$$\frac{p^{d_1}}{p^{d_2}} = \frac{d_2}{d_1}\left[\frac{a^{d_1}}{a^{d_2}}\right] .$$

This equation does not include a term for cavity damping since the only damping contained in it is panel damping. Nevertheless, a knowledge of the damping ratio of the cavity at various cavity depths would be useful to determine. Figure 25, plots the cavity damping ratio at the cavity fundamental depth mode for various cavity depths. Both the experimental damping, and the damping due to the frequency variation with cavity depth are plotted. Note that, unlike the case of panel damping, there is fairly good agreement between experiment and frequency damping, indicating that frequency is the main consideration when computing cavity damping ratios.

Again, as with the panel, Figure 26, plots the variation of cavity pressure with cavity depth for the cases of constant damping effect, frequency damping effect, and experimental damping effect. Recall that the damping ratio used in these calculations are the panel damping ratios and not those of the cavity. Even though cavity damping has not been considered, there is excellent agreement between experiment and the experimental damping case. This indicates

that, for the fundamental cavity depth mode, and the range of cavity depths tested, the use of one-term theory, and only considering panel damping ratios, will predict cavity pressures accurately. The cavity pressures at the higher cavity modes were not measured due to severe coupling of the modes at these higher frequencies.

IV. CONCLUSIONS AND RECOMMENDATIONS

4.1 Conclusions

Based on the experimental work presented in this study, along with the theoretical work presented in Appendix C, the following conclusions can be drawn:

(1) The experimental apparatus used in this study and described in this report is satisfactory for studying sound transmission through a flexible panel into a closed cavity.

(2) The cavity effect on the panel normal mode shapes corresponds to the effects predicted by theory.

(3) Both the cavity stiffness effect and the virtual mass effect are present in a vibrating panel backed by a closed cavity, with the stiffness effect being the main effect on symmetric modes. Also, the stiffness effect is large for the panel fundamental mode and becomes smaller for the higher symmetric modes.

(4) Present one-term theory, as presented by Dowell and Voss,[4] is sufficient to calculate panel frequencies in the range of $\lambda_c a/d$ tested ($\lambda_c a/d \leq 10{,}000$), for $a/d = 2$.

(5) The pressure variation inside the cavity at the panel fundamental frequency and at the cavity fundamental frequency is the same as that predicted by theory.

(6) Panel damping must be taken into account when determining panel deflections and cavity pressures, especially at shallow cavity depths.

(7) Present one-term theory is sufficient to predict panel deflections at the panel fundamental frequency, if the panel damping ratio for that frequency is known. More terms are needed to predict panel deflections at the higher panel frequencies.

(8) Present one-term theory is sufficient to predict cavity pressures at the cavity fundamental, if panel damping is taken into account.

(9) The panel damping ratio of the fundamental mode at various cavity depths does not vary with frequency in the same manner as the panel damping ratio in various panel modes at fixed cavity depth (so-called "frequency damping"); however, the cavity damping ratios may be accurately predicted from such a model.

4.2 Recommendations

Based on the studies contained in this report, it is recommended that further research be performed in three basic research areas:

(1) A further investigation into the response of a panel and a cavity to sinusoidal excitation, with special emphasis on the experimental determination and theoretical predictions of panel and cavity damping ratios. This study

could be combined with further computer calculations to determine panel deflections and cavity pressures at higher frequencies, along with investigation of these higher, more densely spaced, modes.

(2) A complication of the problem discussed in this report, by using random noise excitation for the external acoustic field. The use of random noise could more closely predict the response of an airfoil to boundary layer turbulence. Since a random noise generator can be used to emit "white noise", i.e., noise with a constant power spectra, a comparison between theory and experiment would be easier than reducing the more random data of wind tunnel results. Some exploratory work has been performed by the author in this area. Preliminary results seem to indicate that the response spectra for the panel and cavity are similar to those given in Figures 8 and 9. Further work at shallow cavity depths is needed to check the sinusoidal results.

(3) The use of perhaps a sawtooth generator to approximate a sonic boom time signature, or "N-wave". A study of this type would mainly be an investigation of the transient behavior of the panel and cavity. Such a study could be used to predict the response of a structure to a sonic boom without the problems of a complex pressure wave generating device.[18] The use of a more complex structure with perhaps openings or two flexible walls could be used

with such an "N-wave" excitation to investigate the response of buildings more exactly.

REFERENCES

1. Morse, P. M. and Ingard, K. V., Theoretical Acoustics, McGraw-Hill Co., Inc., 1968.

2. Carden, H. D., Findley, D. S. and Mayes, W. H., "Building Vibrations Due to Aircraft Noise and Sonic Boom Excitation", ASME 69-WA/GT-8, 1969.

3. Carden, H. D. and Mayes, W. H., "Measured Vibration Response Characteristics of Four Residential Structures Excited by Mechanical and Acoustical Loadings", NASA TN D-5776, April 1970.

4. Dowell, E. H. and Voss, H. M., "Experimental and Theoretical Panel Flutter Studies in the Mach Number Range of 1.0 to 5.0", Air Force Flight Dynamics Lab., ASD-TDR-63-449, December 1963.

5. Pretlove, A. J. and Craggs, A., "A Simple Approach to Coupled Panel-Cavity Vibrations", J. Sound Vib., 11, pp. 207-215, 1970.

6. Dowell, E. H. and Voss, H. M., "The Effect of a Cavity on Panel Vibration", AIAA Journal, 1, p. 476, 1963.

7. Pretlove, A. J., "Free Vibrations of a Rectangular Panel Backed by a Closed Rectangular Cavity", J. Sound and Vib., 2, pp. 197-209, 1965.

8. Pretlove, A. J., "Forced Vibrations of a Rectangular Panel Backed by a Closed Rectangular Cavity", J. Sound and Vib., 3, pp. 252-261, 1966.

9. Dugundji, J.: Errata and Addenda: "Theoretical Considerations of Panel Flutter at High Supersonic Mach Numbers", AIAA Journal, 7, p. 1663, 1969.

10. Sheshadri, T. V., "Transient Response of Mechano-Acoustical Networks", Ph.D. Thesis, Oklahoma State University, 1968.

11. Bolotin, V. V., Nonconservative Problems of the Theory of Elastic Stability, MacMillan Co., New York, 1963.

12. Dowell, E. H., "Transmission of Noise From a Turbulent Boundary Layer Through a Flexible Plate into a Closed Cavity", J. Acoust. Soc. Am., 46, pp. 238-252, July 1969.

13. Moore, J. A., "Response of Flexible Panels to Turbulent Boundary Layer Excitation", M.I.T. Acoustics and Vibration Laboratory, Report No. 70208-3, July 1969.

14. Dowell, E. H., "Noise or Flutter or Both?", Presented at the British Acoustical Society Meeting "Sonically Induced Vibration of Structures", January 1969.

15. Ventres, C. S., "Cavity Response to Arbitrary Motions of a Flexible Wall", Personal Communication, 1970.

16. Housner, G. W. and Hudson, D. E., Applied Mechanics Dynamics, D. Van Nostrand Co., Inc., 1959.

17. Warburton, G. B., "The Vibration of Rectangular Plates", Proc. Inst. Mech. Engrs. (London), 168, pp. 371-384, 1954.

18. Craggs, A., "Short Course in Acoustics and Noise", Inst. of Sound and Vib. Research, The University, Southampton, 1968.

19. Lord Rayleigh, Theory of Sound (two volumes), Dover Publications, New York, Second Edition, 1945 re-issue, 1955.

20. Timoshenko, S., Vibration Problems in Engineering, D. Van Nostrand Co., 1955.

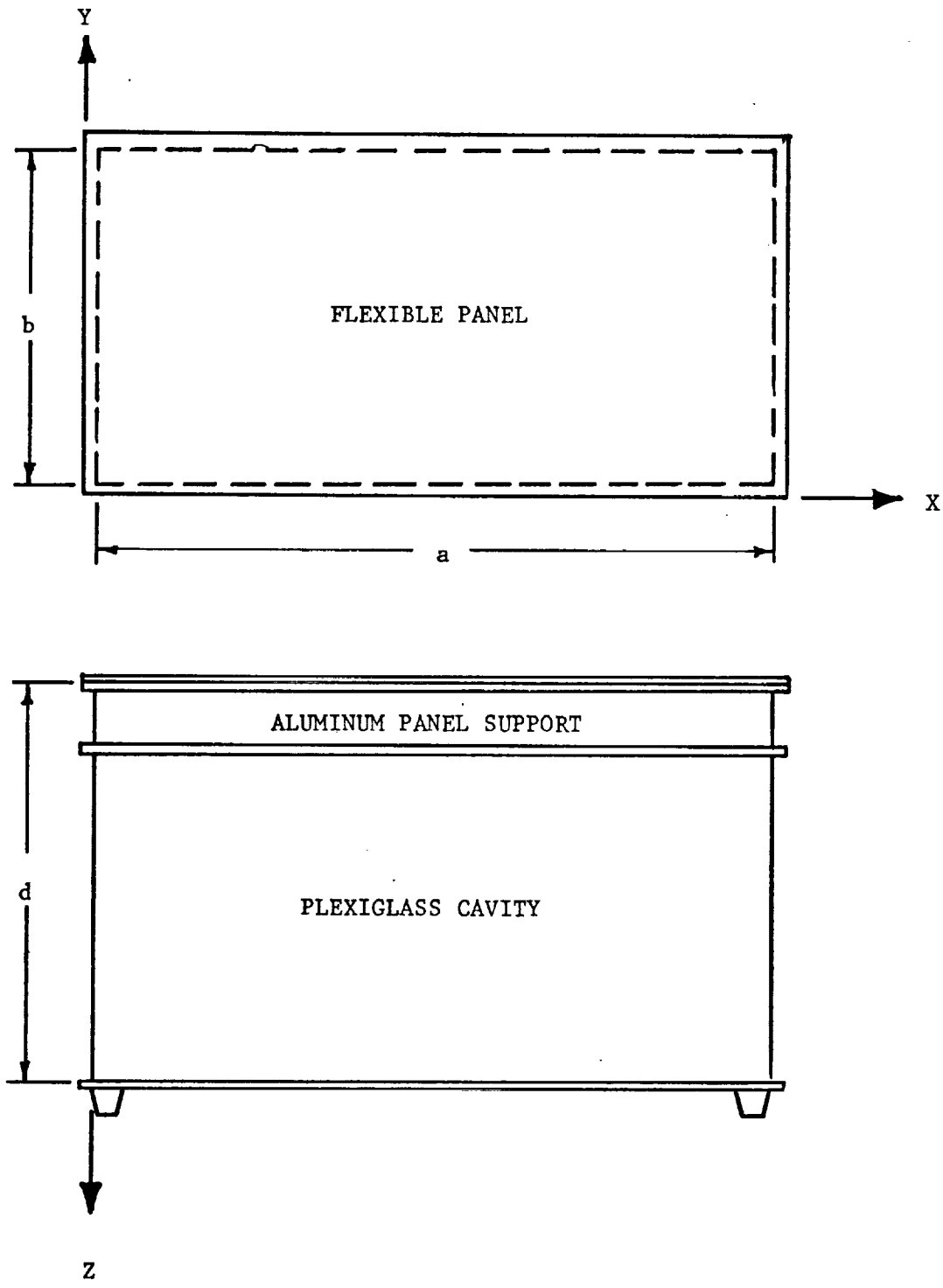

CAVITY - PANEL GEOMETRY

Figure 1

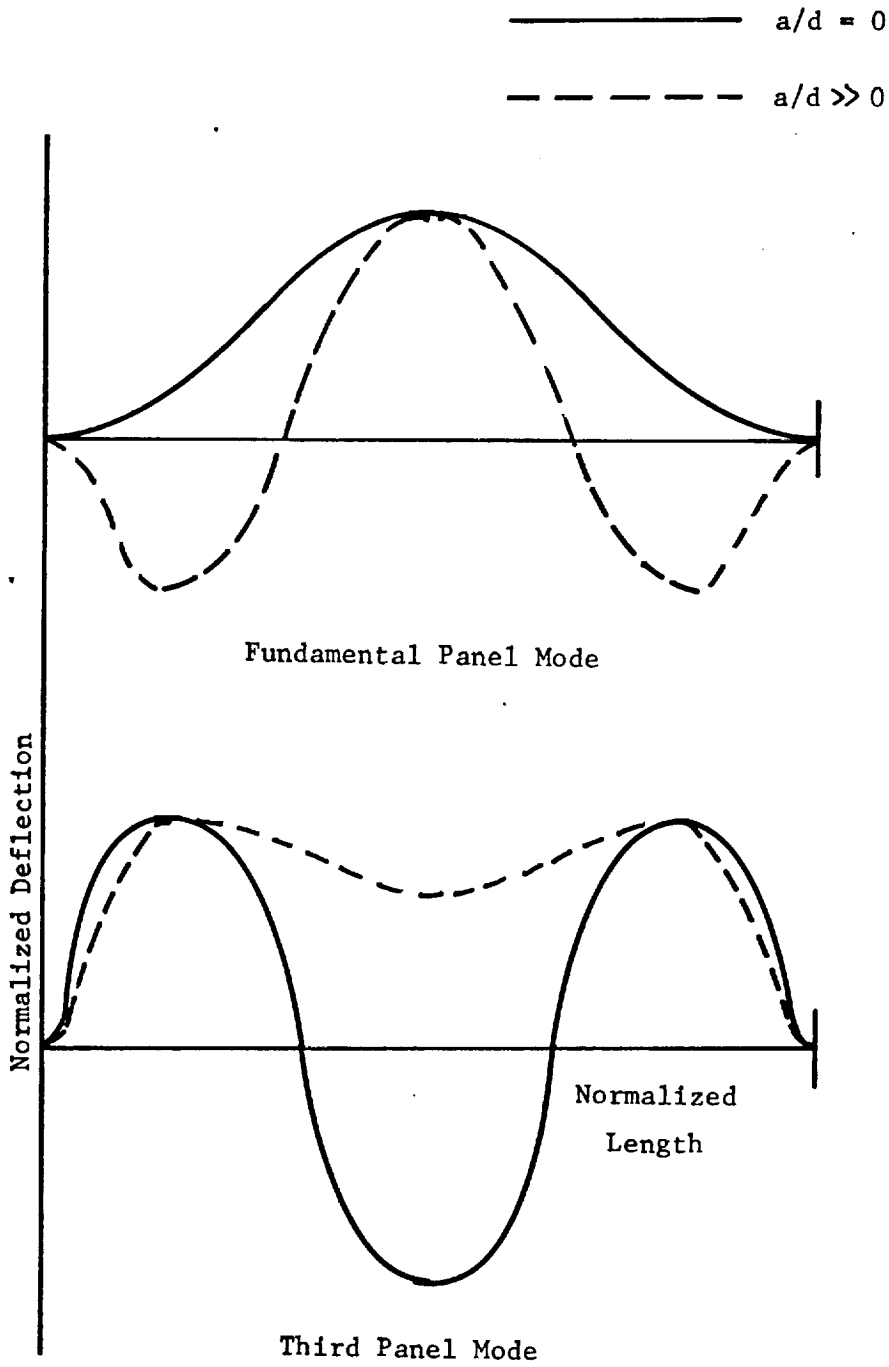

CAVITY EFFECT ON PANEL NORMAL MODE SHAPES

Figure 2

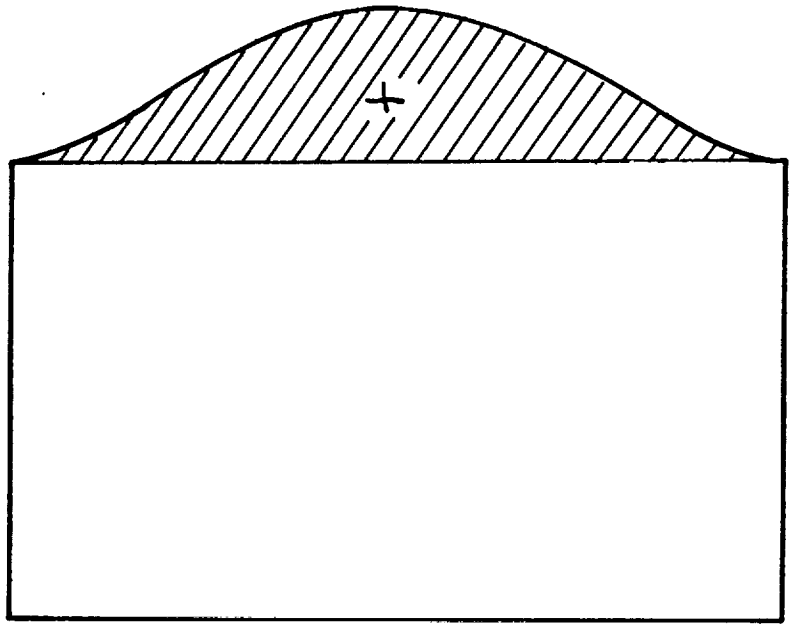

Fundamental Mode

Figure 3

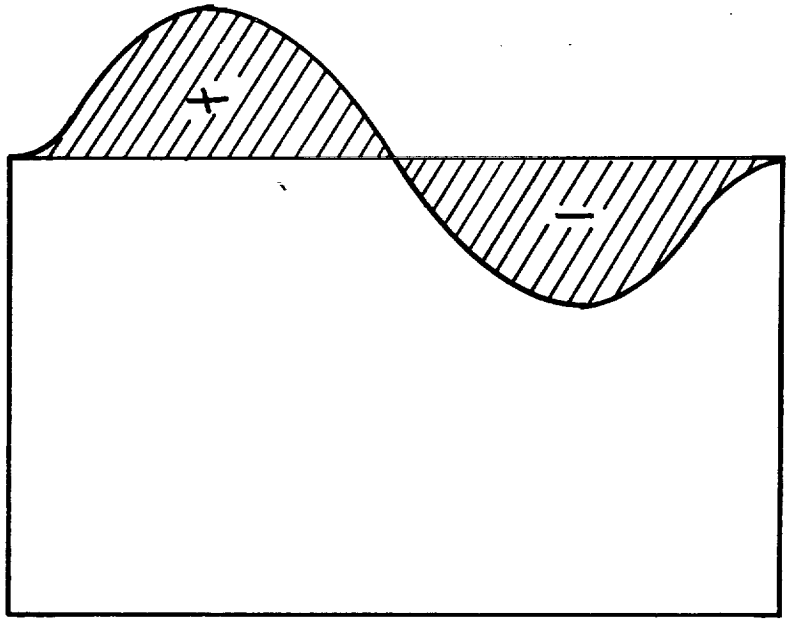

Second Mode

Figure 4

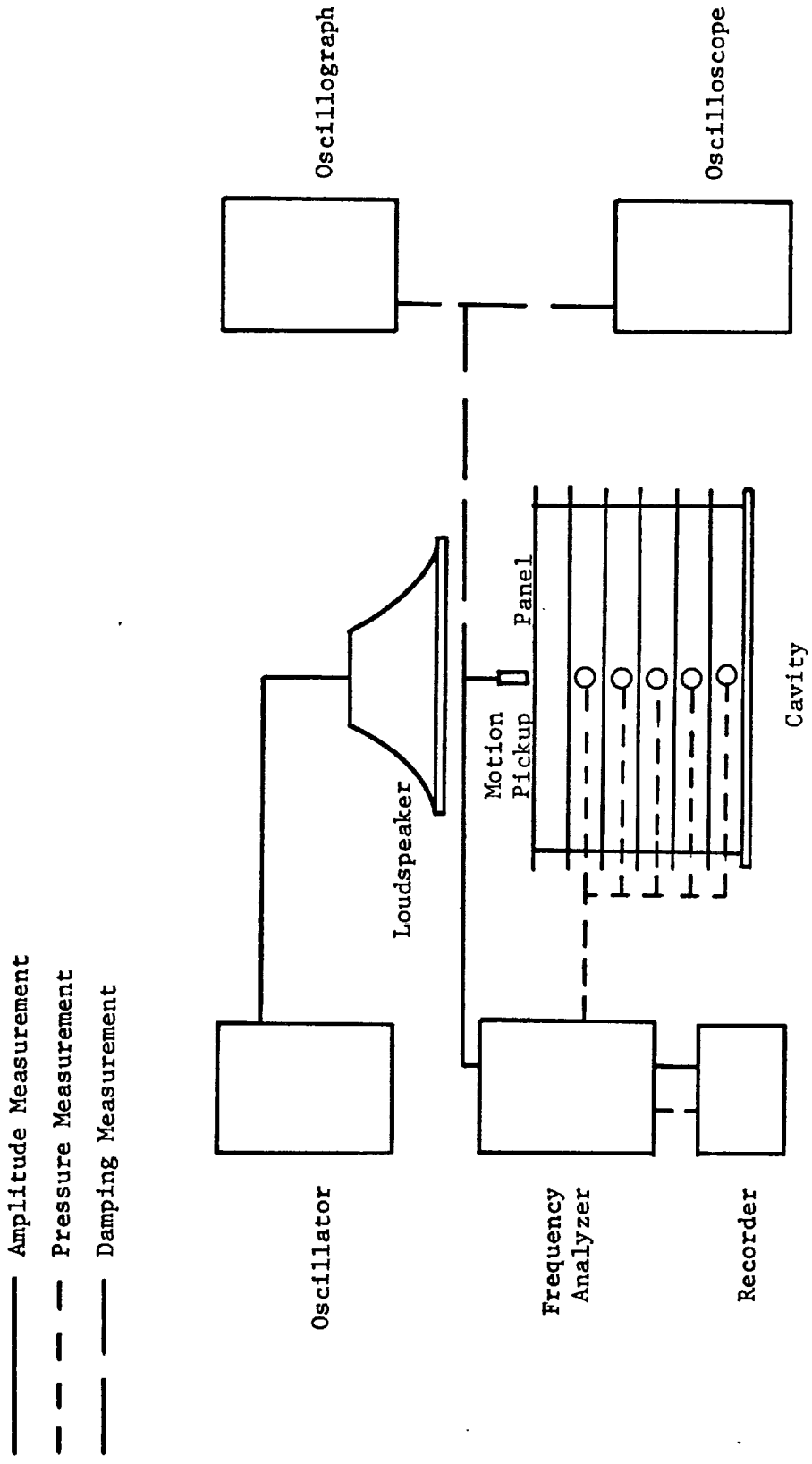

EXPERIMENTAL ARRANGEMENT

Figure 5

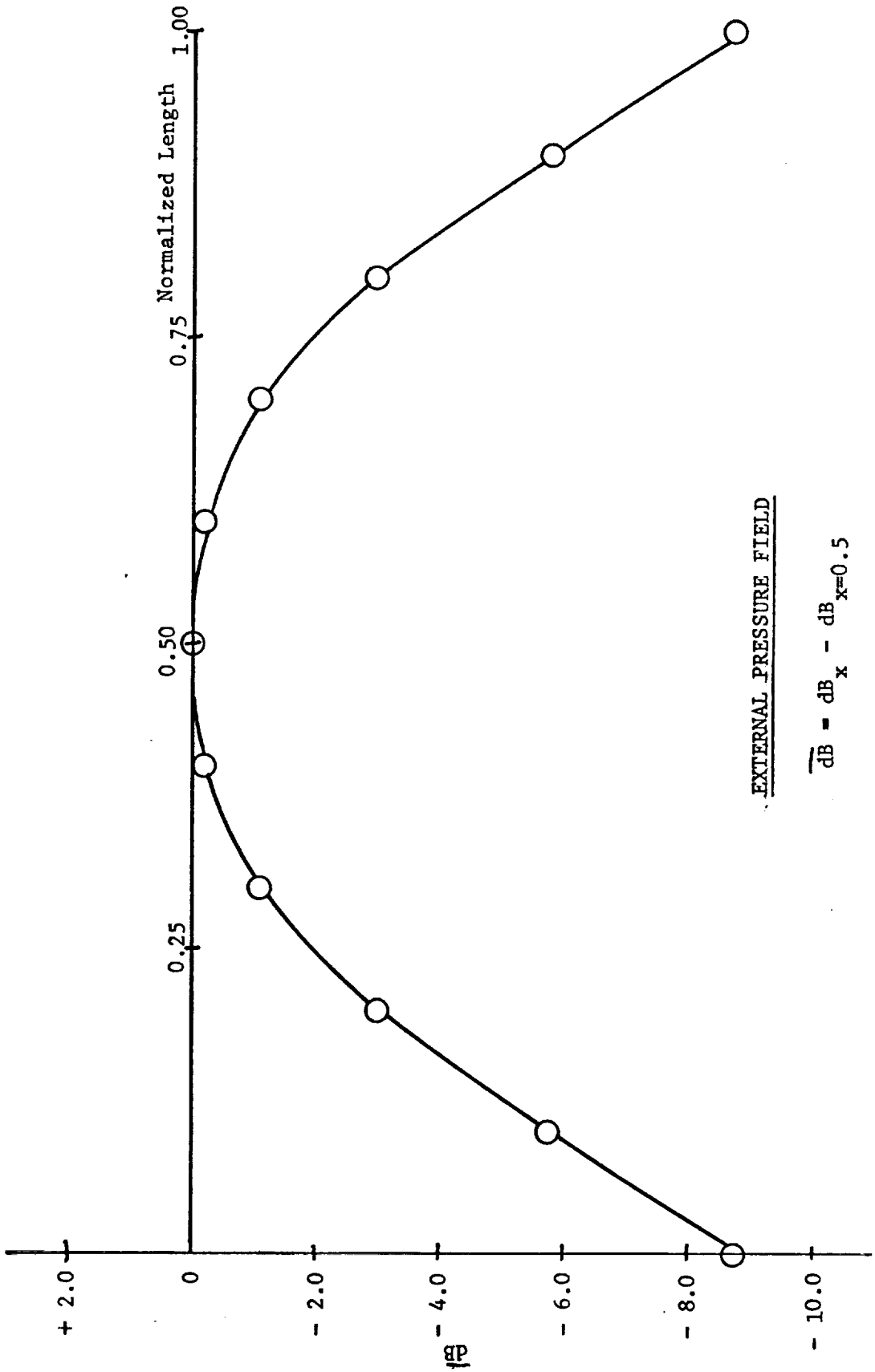
Normalized Length
0.25
0.50
0.75
1.00
+ 2.0
0
- 2.0
- 4.0
- 6.0
- 8.0
- 10.0
dB
EXTERNAL PRESSURE FIELD
$\overline{dB} = dB_x - dB_{x=0.5}$

Figure 6

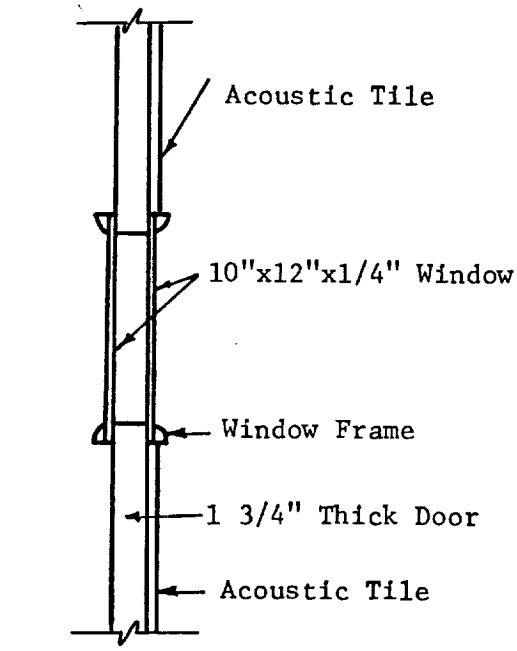

WINDOW SECTION

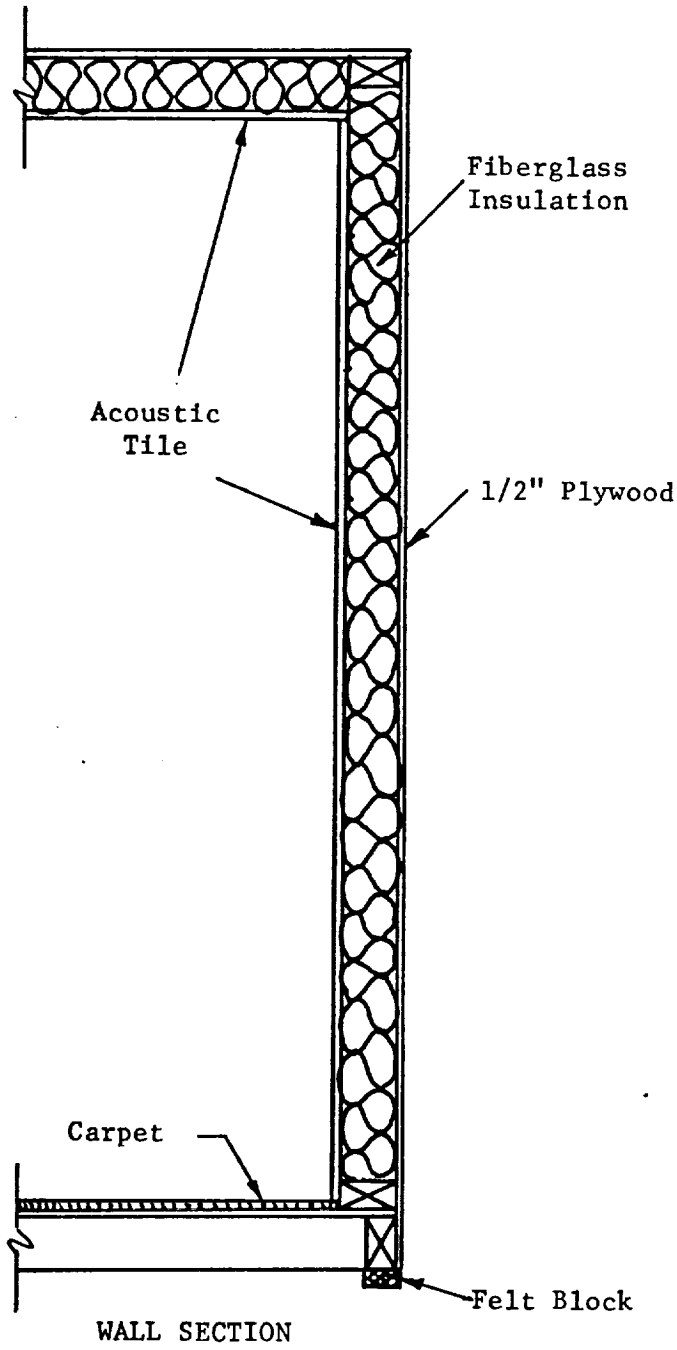

WALL SECTION

TYPICAL ACOUSTIC CHAMBER SECTIONS

Figure 7

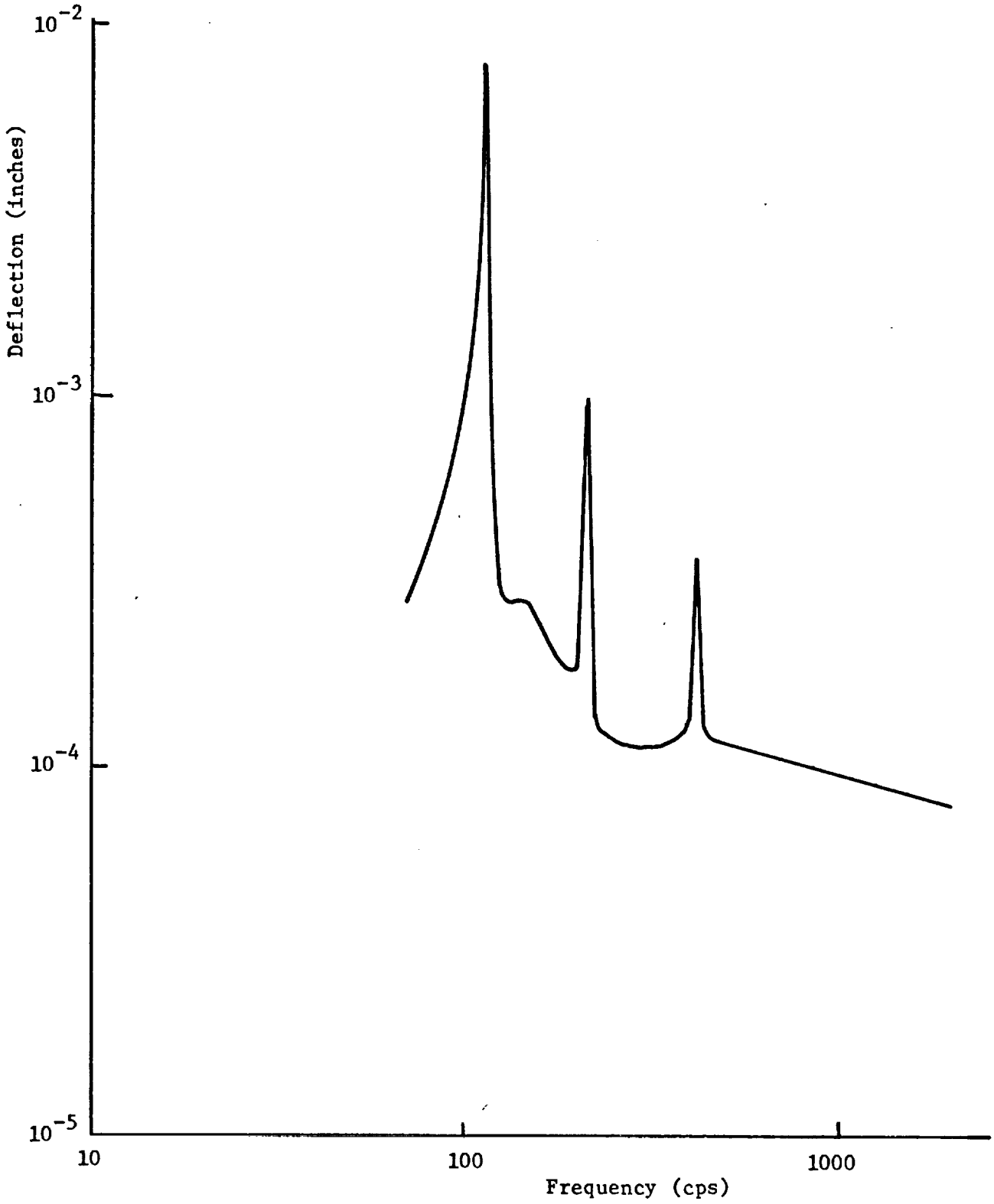

PANEL RESPONSE TO SINUSOIDAL EXTERNAL FIELD

Figure 8

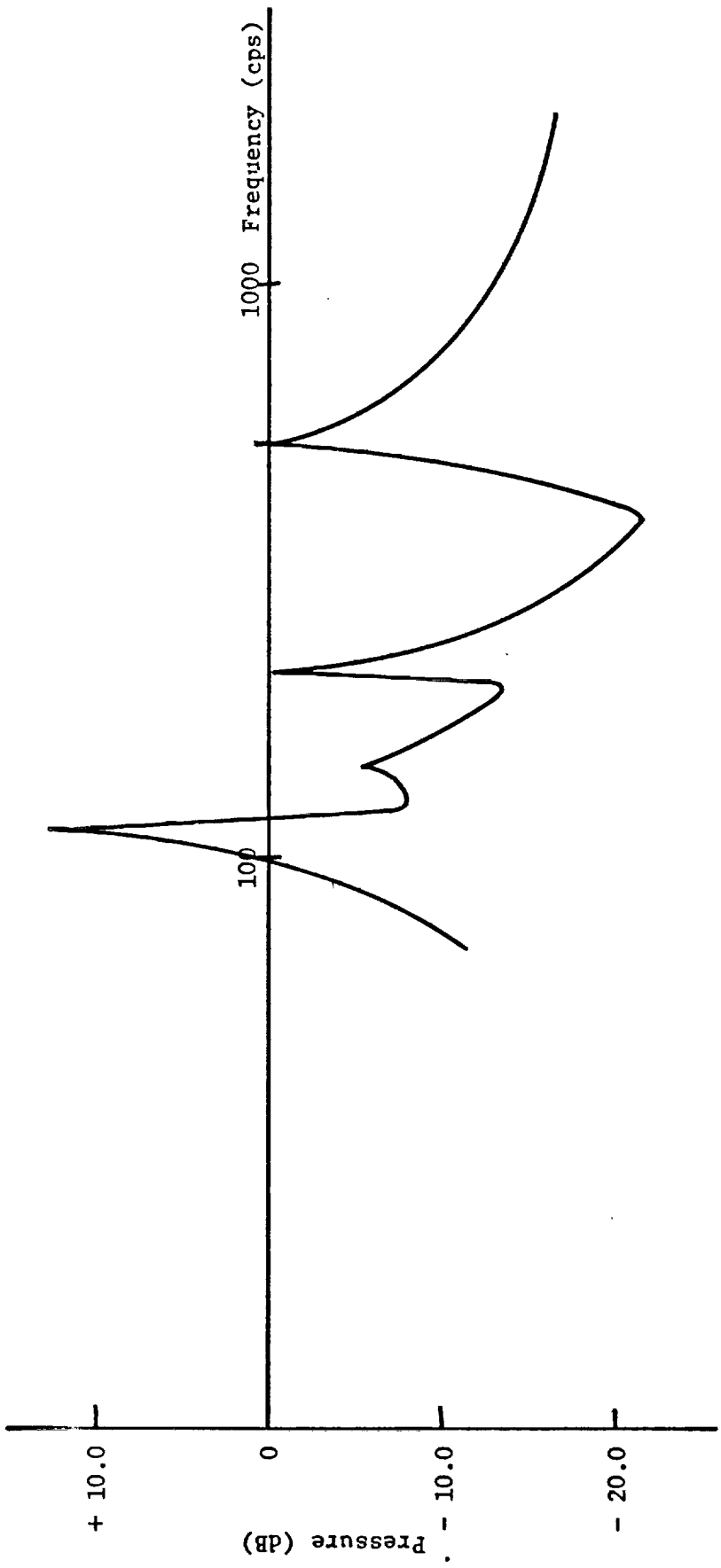

CAVITY RESPONSE TO SINUSOIDAL EXTERNAL FIELD

Figure 9

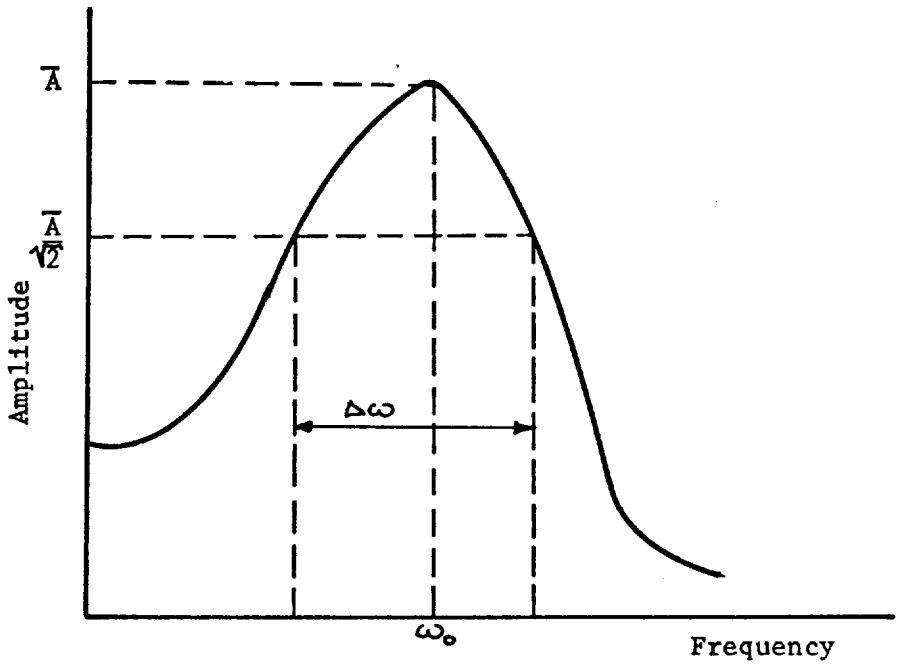

DAMPING RATIO VIA PEAK METHOD

Figure 10a

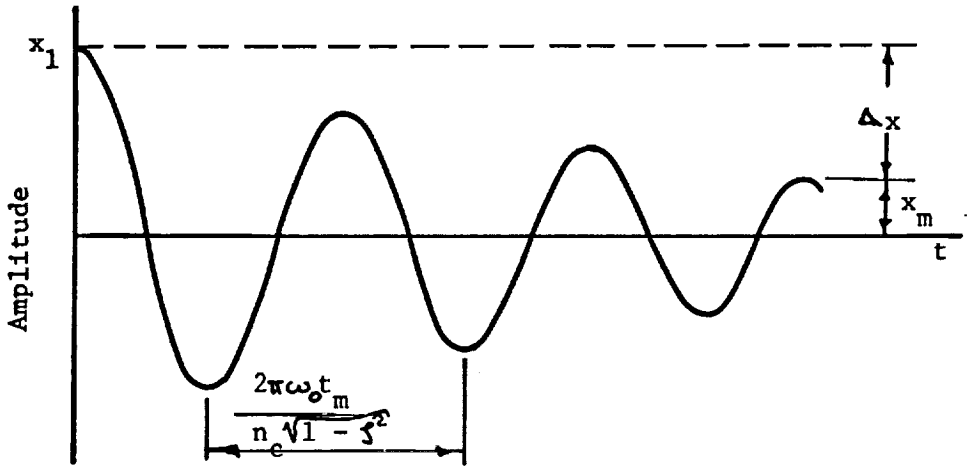

DAMPING RATIO VIA DECAY METHOD

Figure 10b

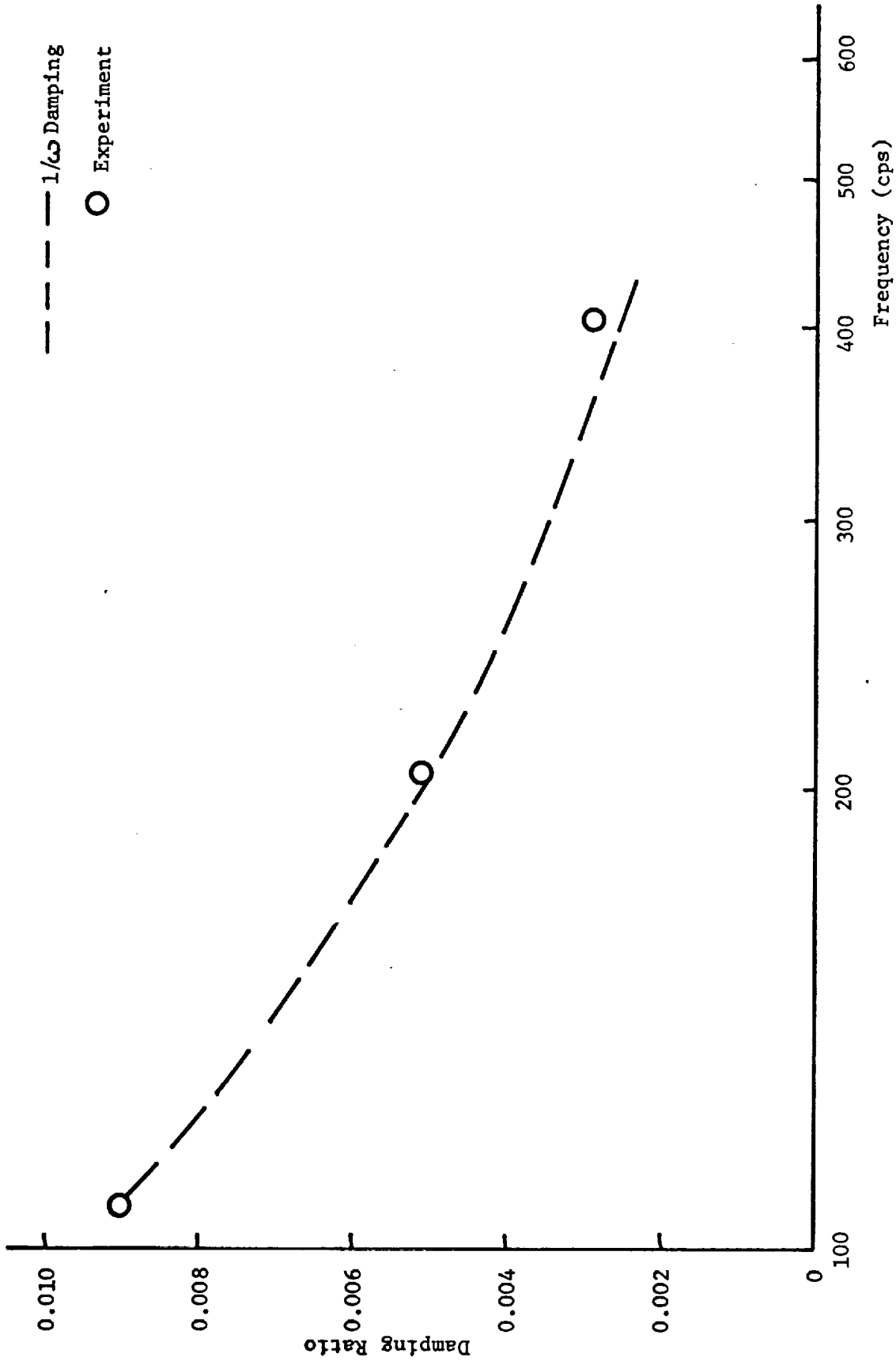

PANEL DAMPING VS. FREQUENCY

Figure 11

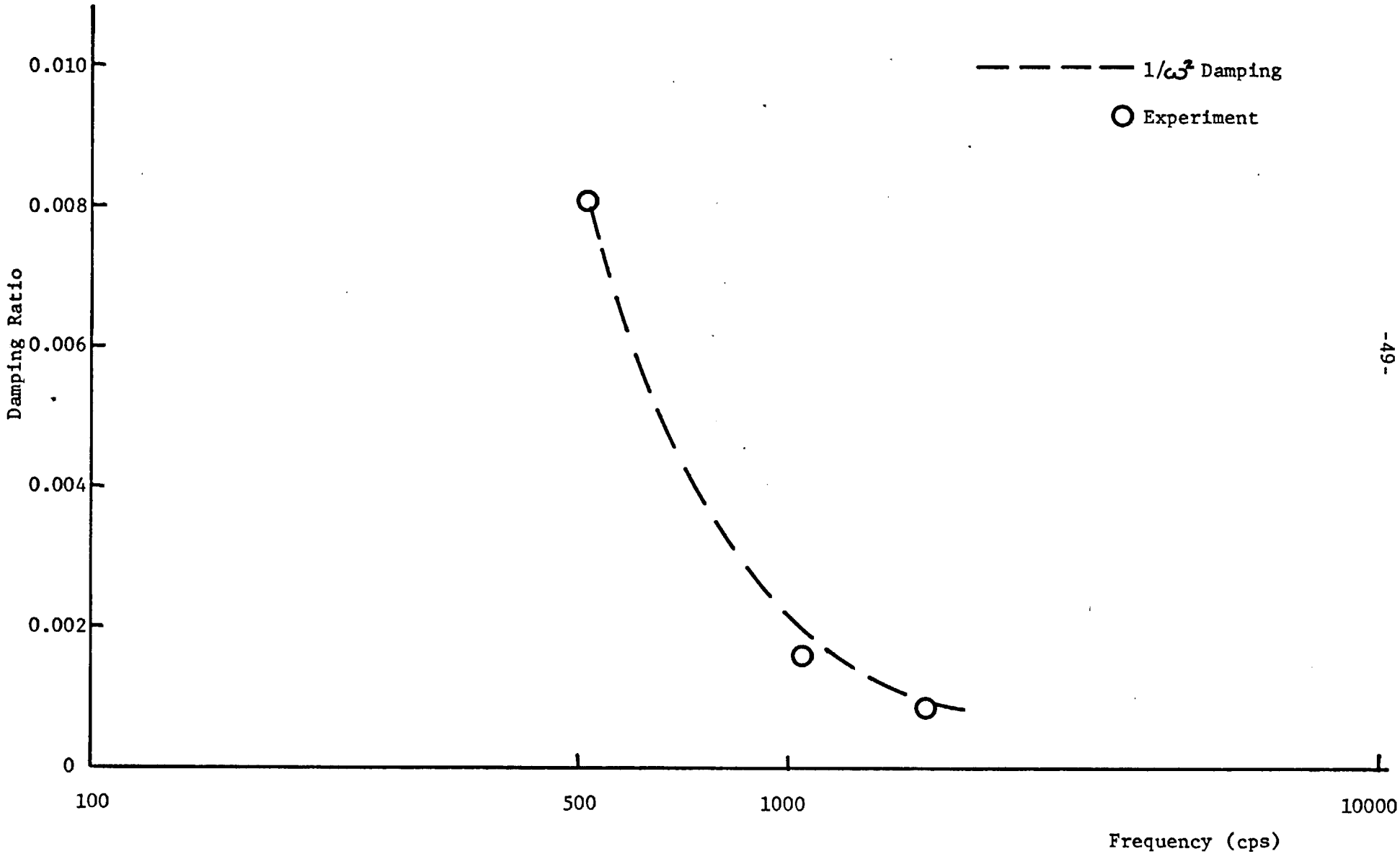

CAVITY DAMPING VS. FREQUENCY

Figure 12

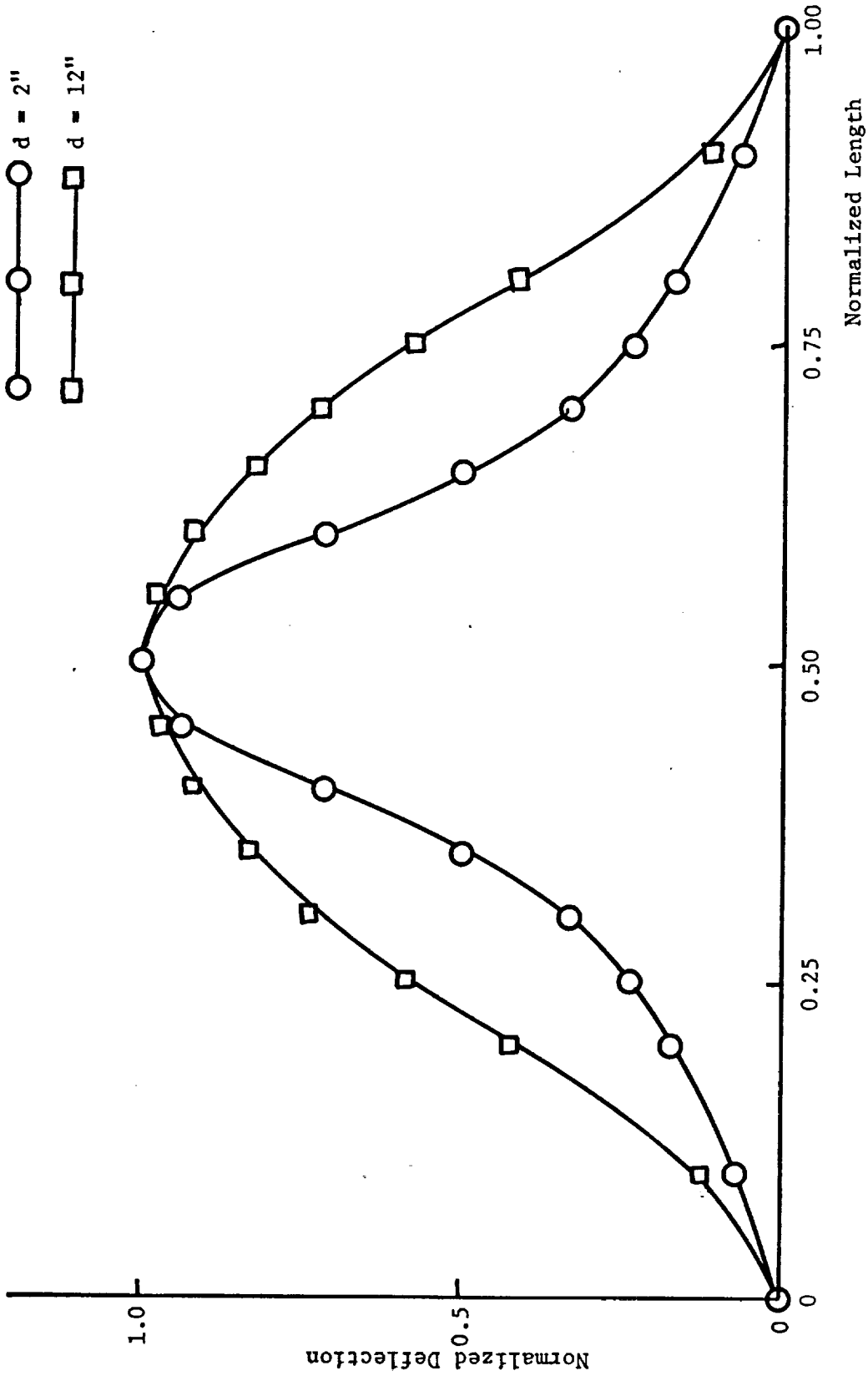

CAVITY EFFECT ON PANEL NORMAL MODE SHAPES
(Fundamental Mode)

Figure 13

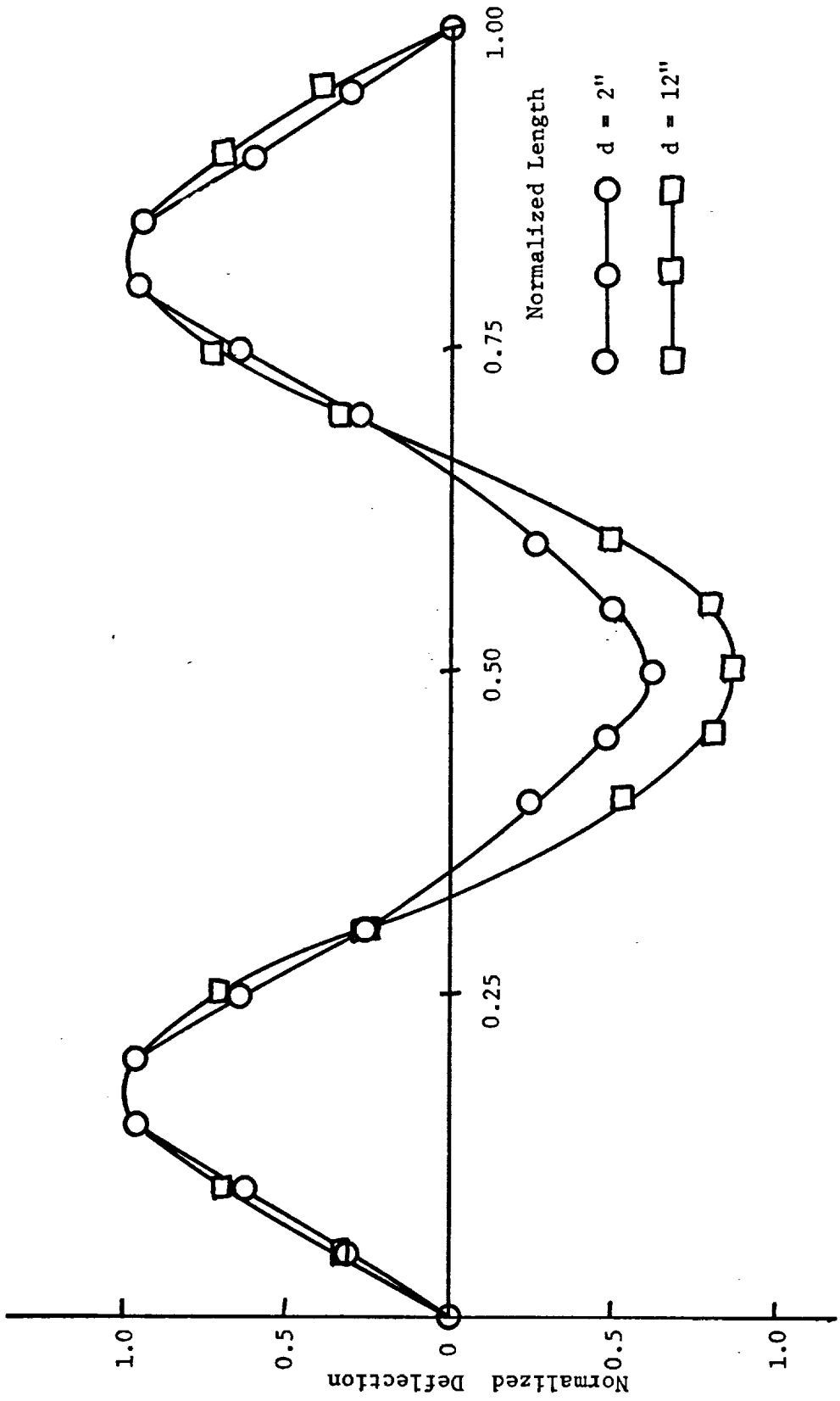

CAVITY EFFECT ON PANEL NORMAL MODE SHAPES
(Third Mode)

Figure 14

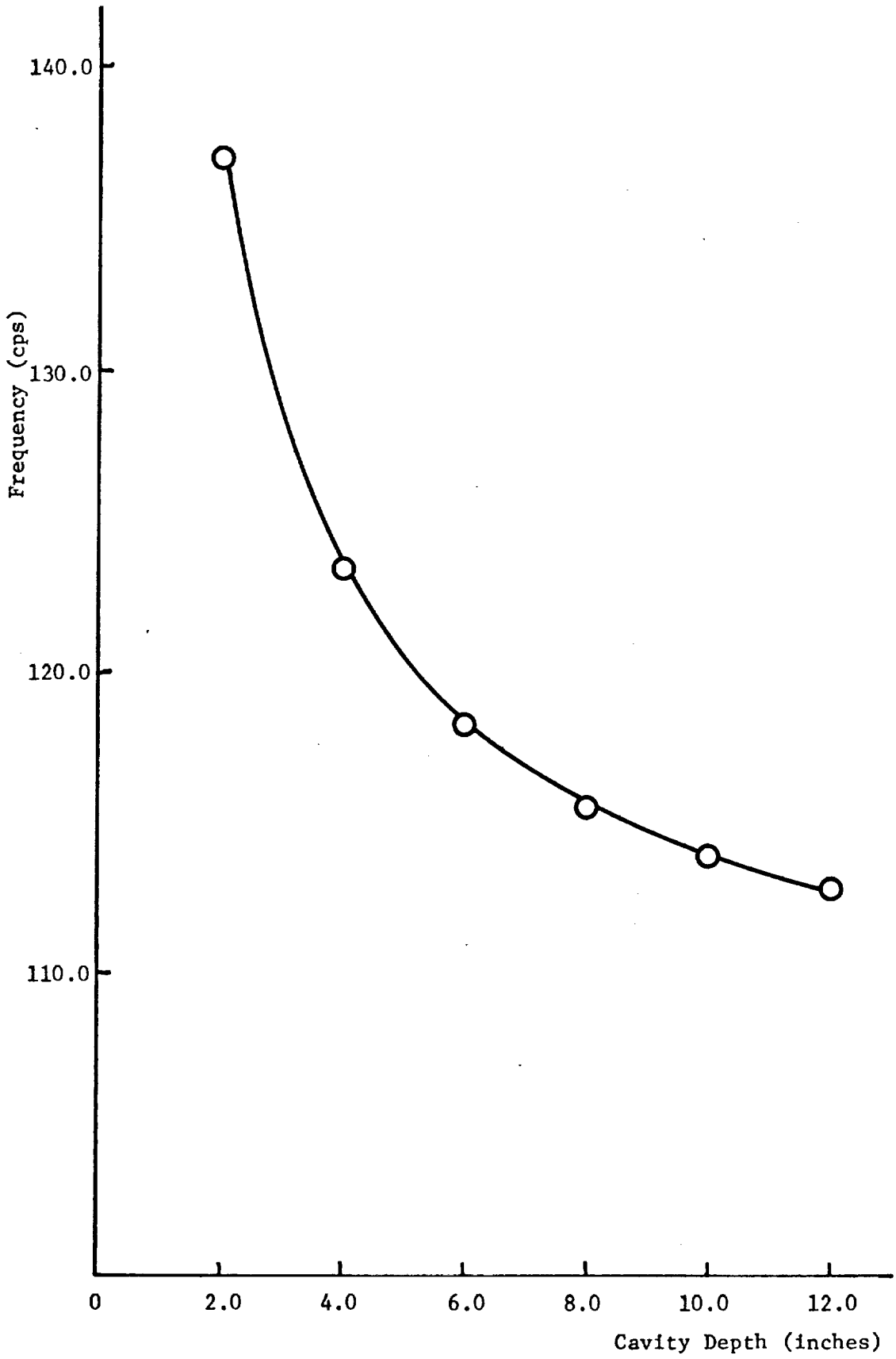

FUNDAMENTAL PANEL FREQUENCY VS. CAVITY DEPTH

Figure 15

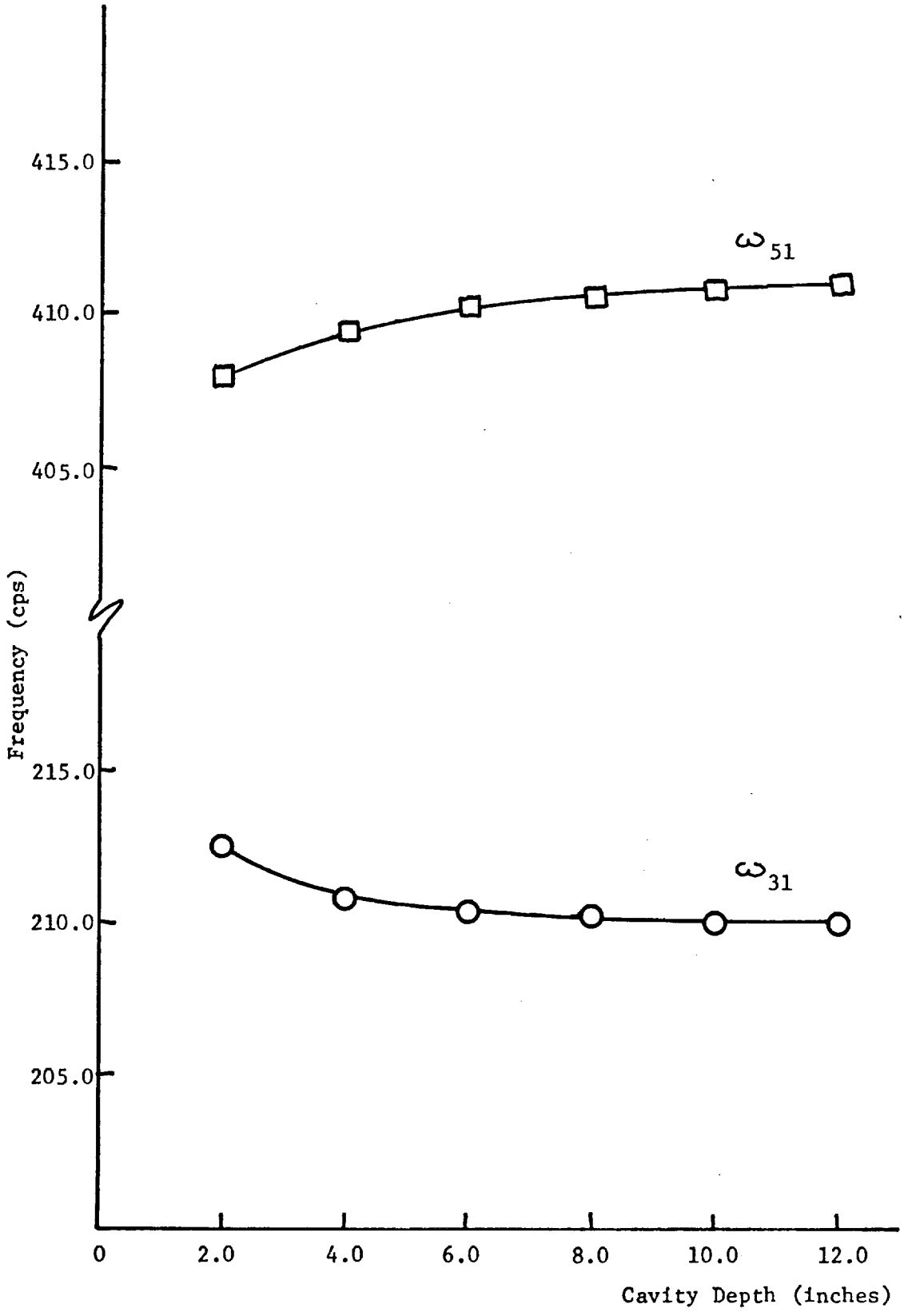

THIRD AND FIFTH PANEL FREQUENCY VS. CAVITY DEPTH

Figure 16

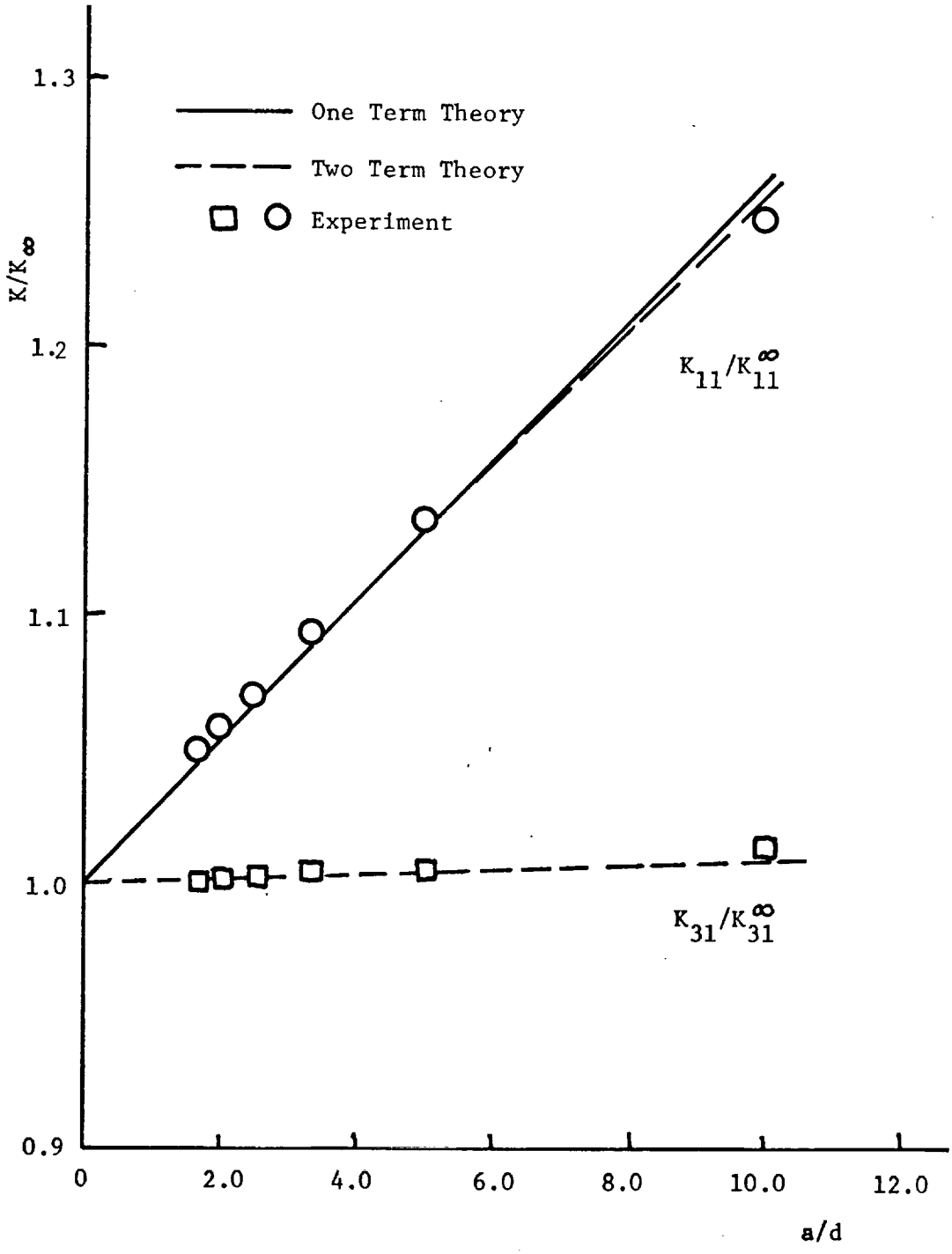

CAVITY EFFECT ON PANEL NATURAL FREQUENCIES

Figure 17

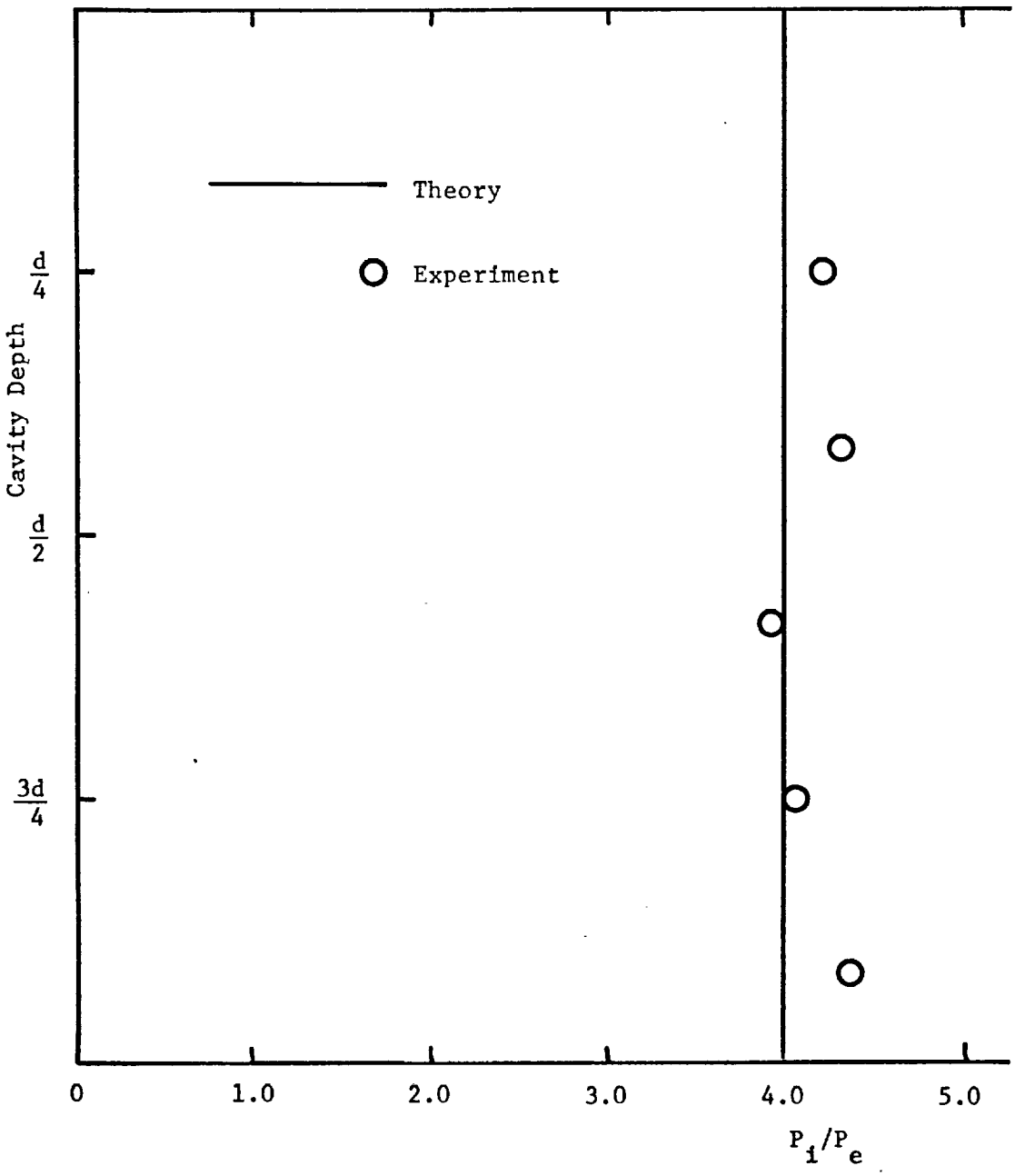

PRESSURE DISTRIBUTION

(at panel fundamental)

Figure 18

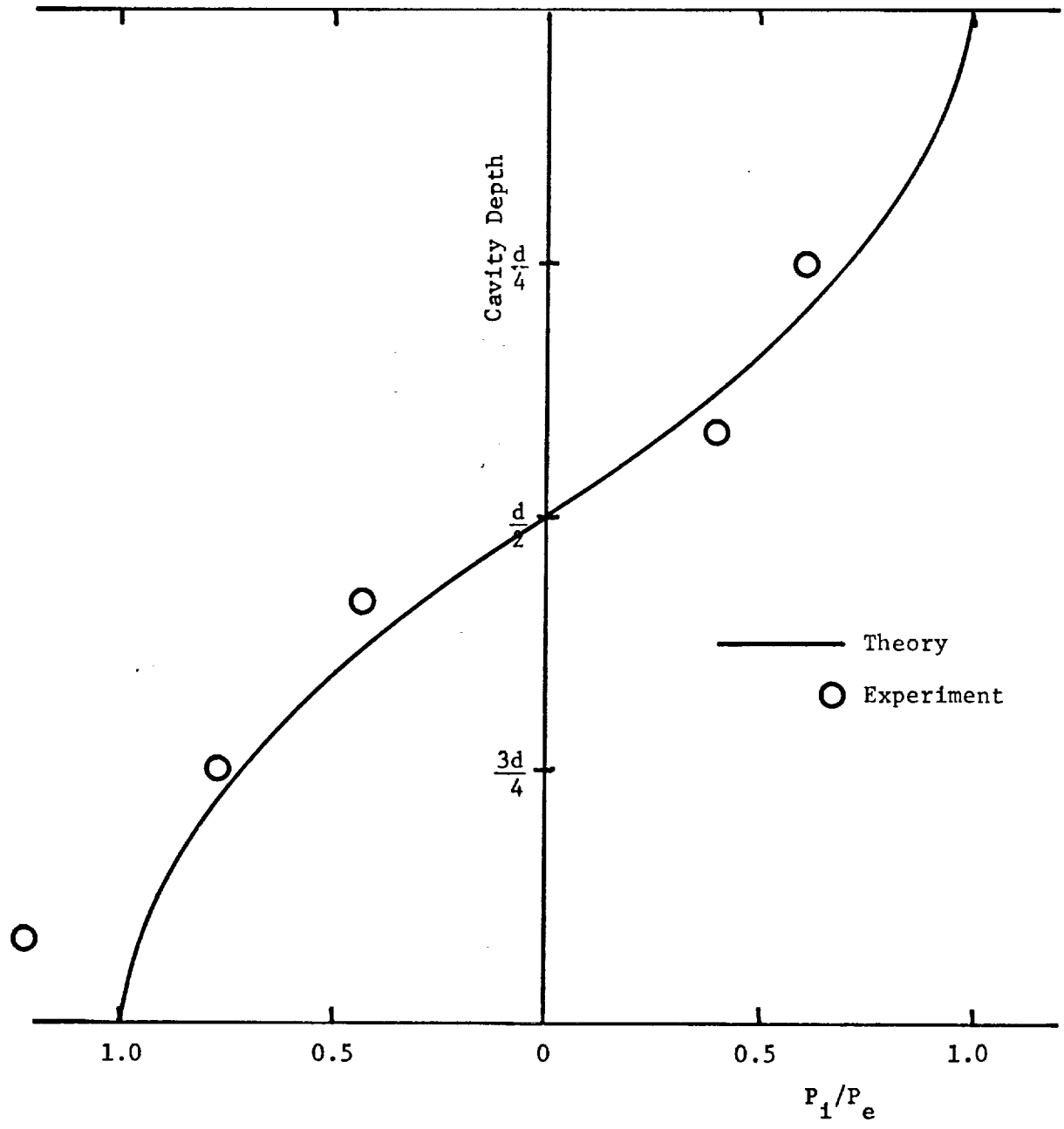

PRESSURE DISTRIBUTION

(at cavity fundamental)

Figure 19

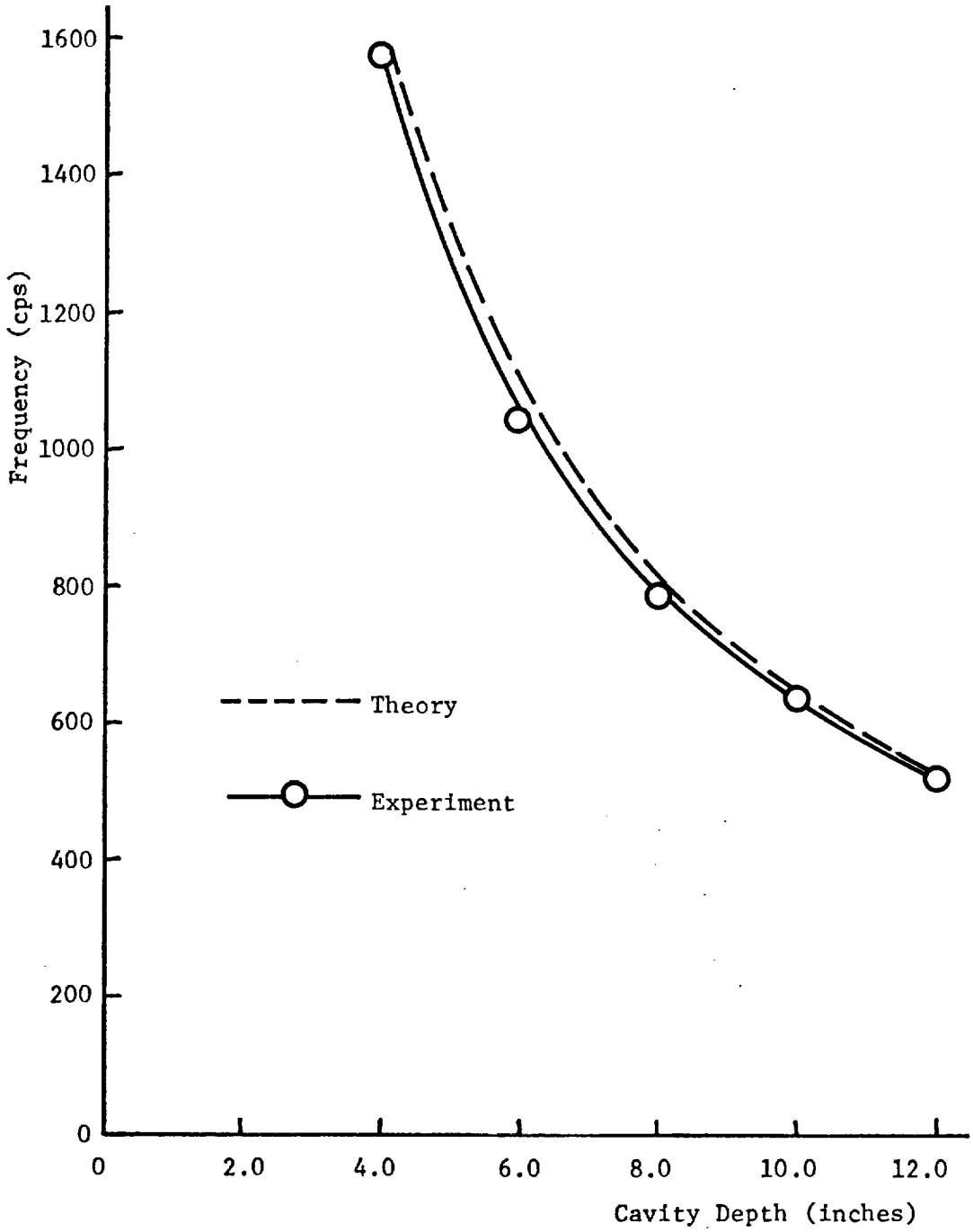

CAVITY FUNDAMENTAL FREQUENCY VS. CAVITY DEPTH

Figure 20

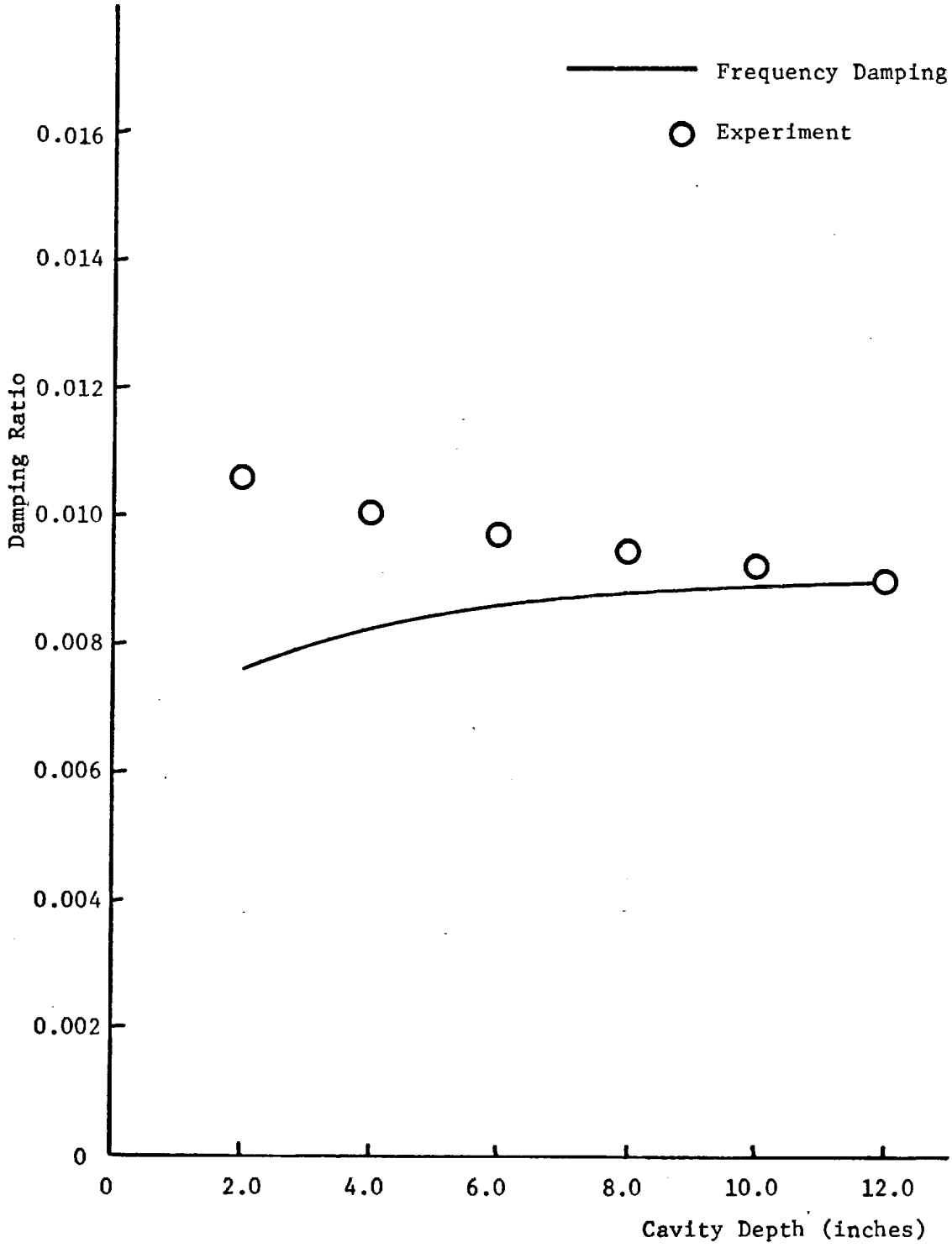

PANEL DAMPING RATIO VS. CAVITY DEPTH

(Panel Fundamental Mode)

Figure 21

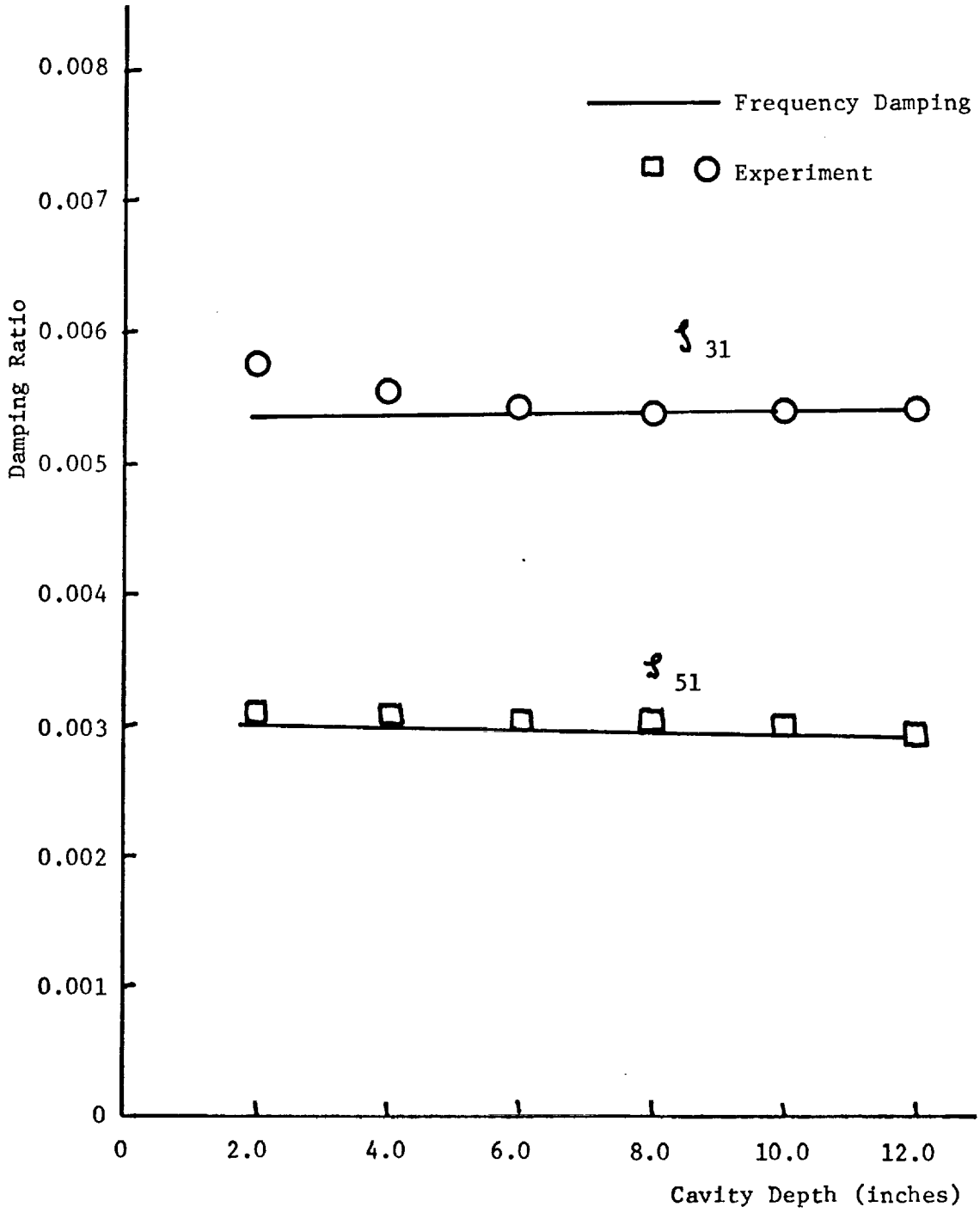

PANEL DAMPING RATIO VS. CAVITY DEPTH

(Third and Fifth Panel Modes)

Figure 22

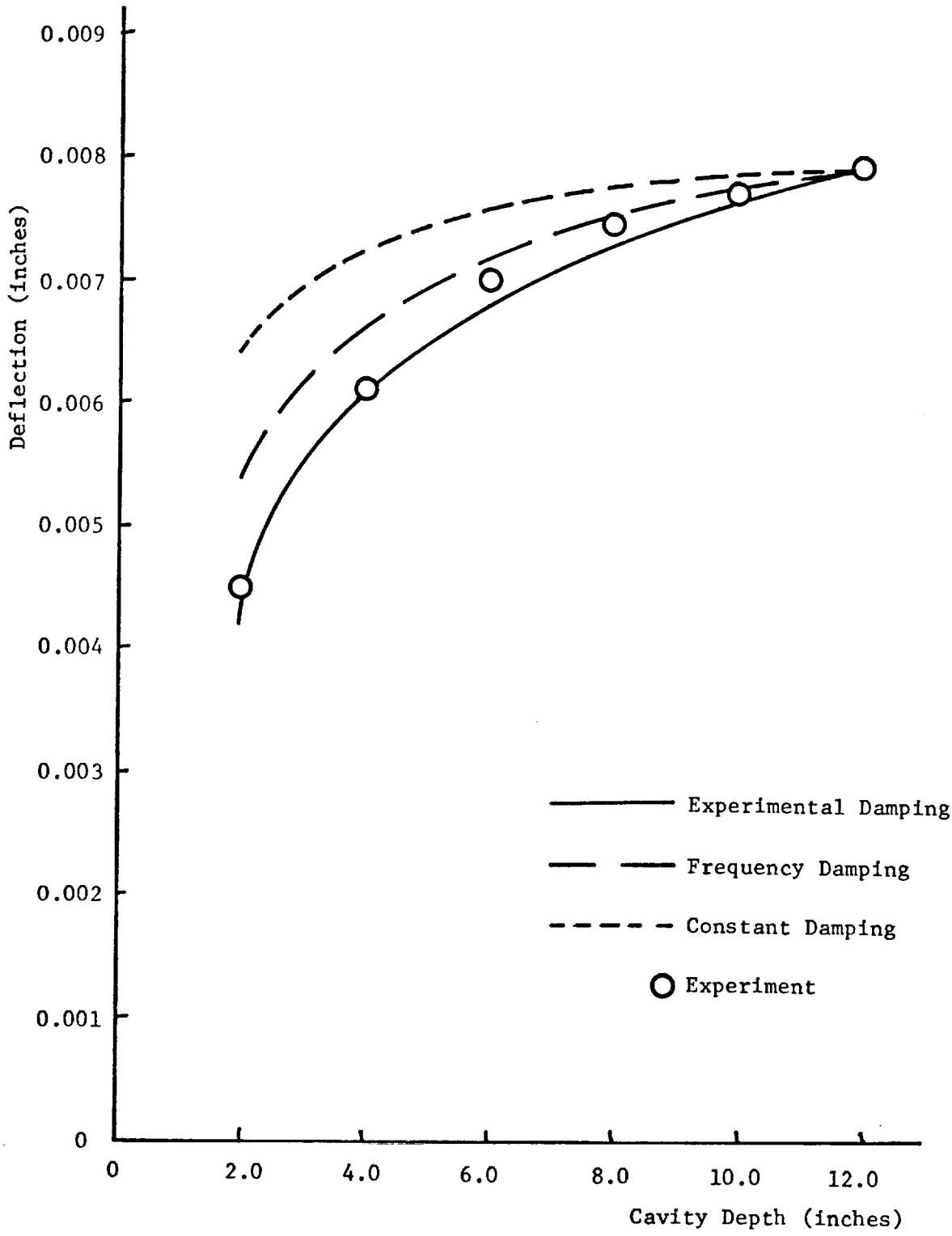

PANEL DEFLECTION VS. CAVITY DEPTH

(Panel Fundamental Mode)

Figure 23

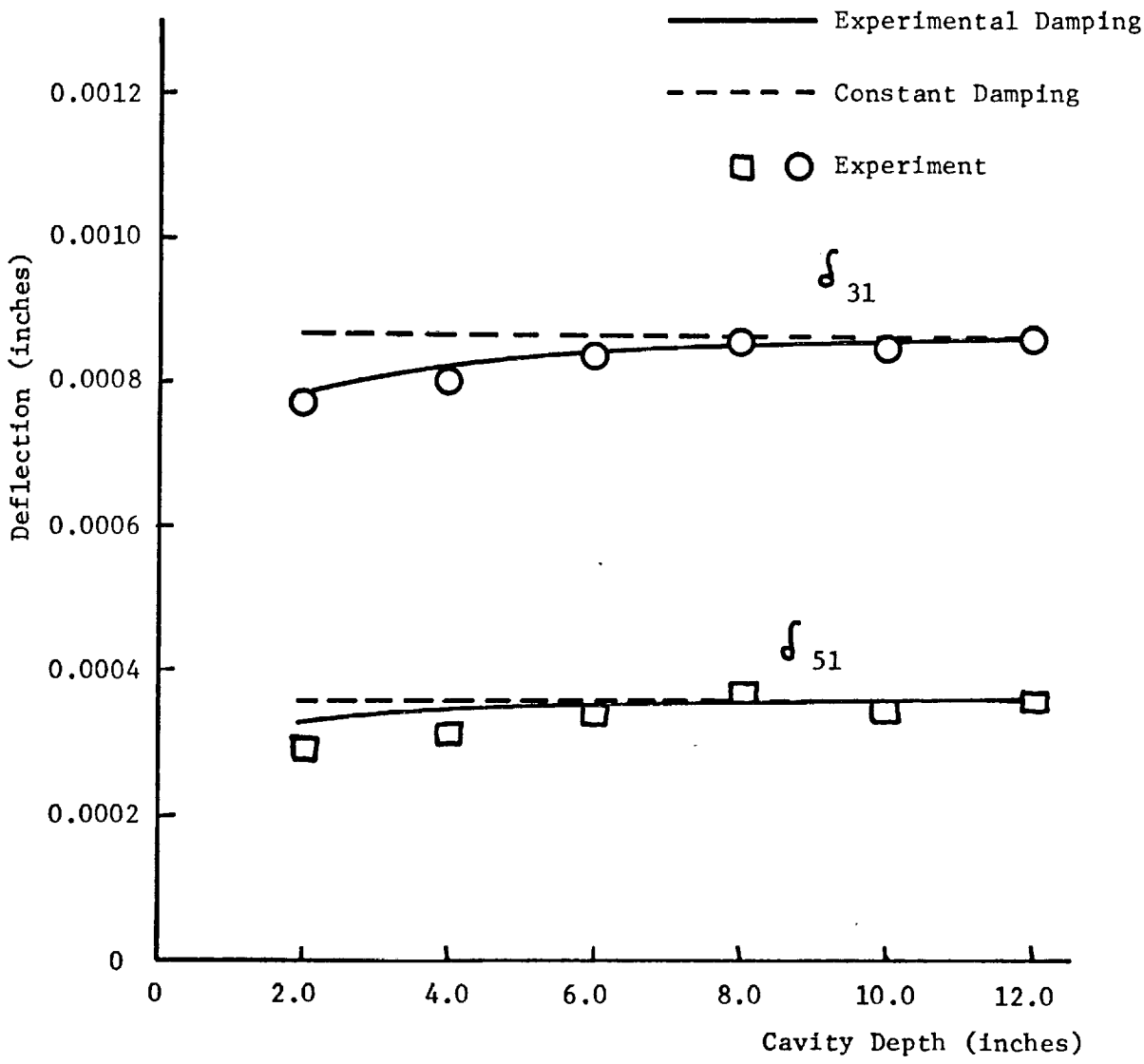

PANEL DEFLECTION VS. CAVITY DEPTH

(Third and Fifth Panel Modes)

Figure 24

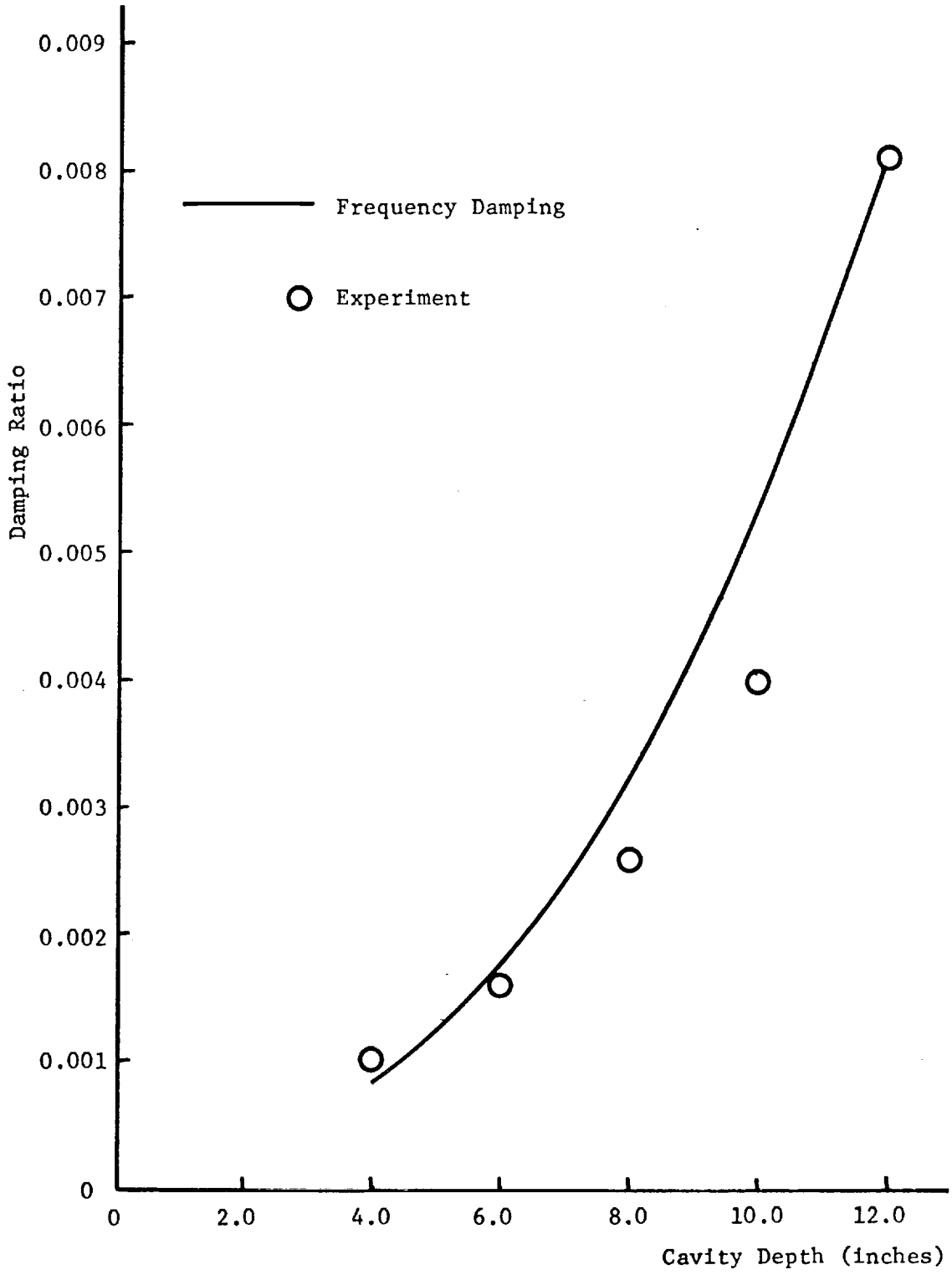

CAVITY DAMPING RATIO VS. CAVITY DEPTH

Figure 25

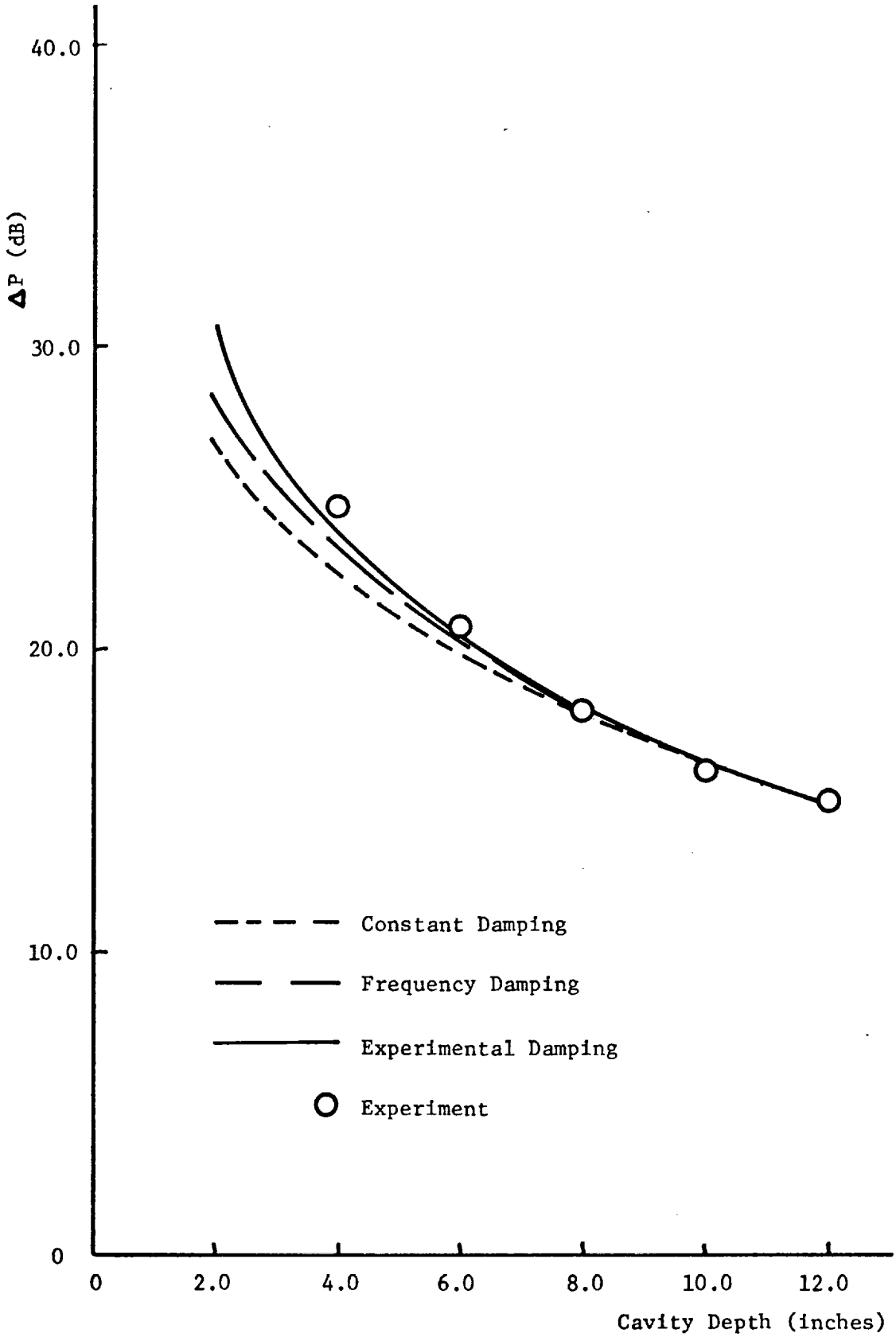

CAVITY PRESSURE VS. CAVITY DEPTH

Figure 26

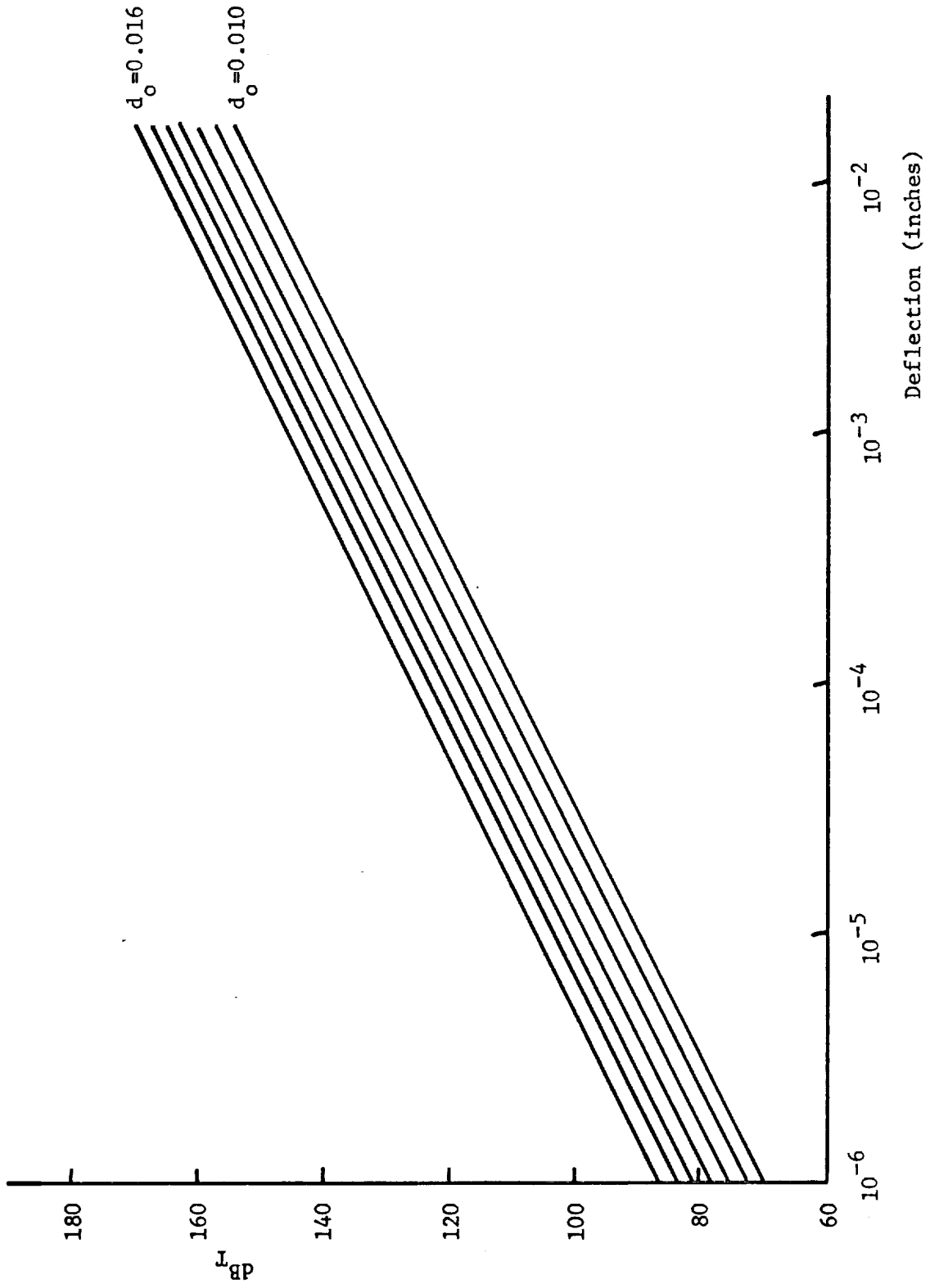

RECORDER - PANEL CALIBRATION

Figure 27

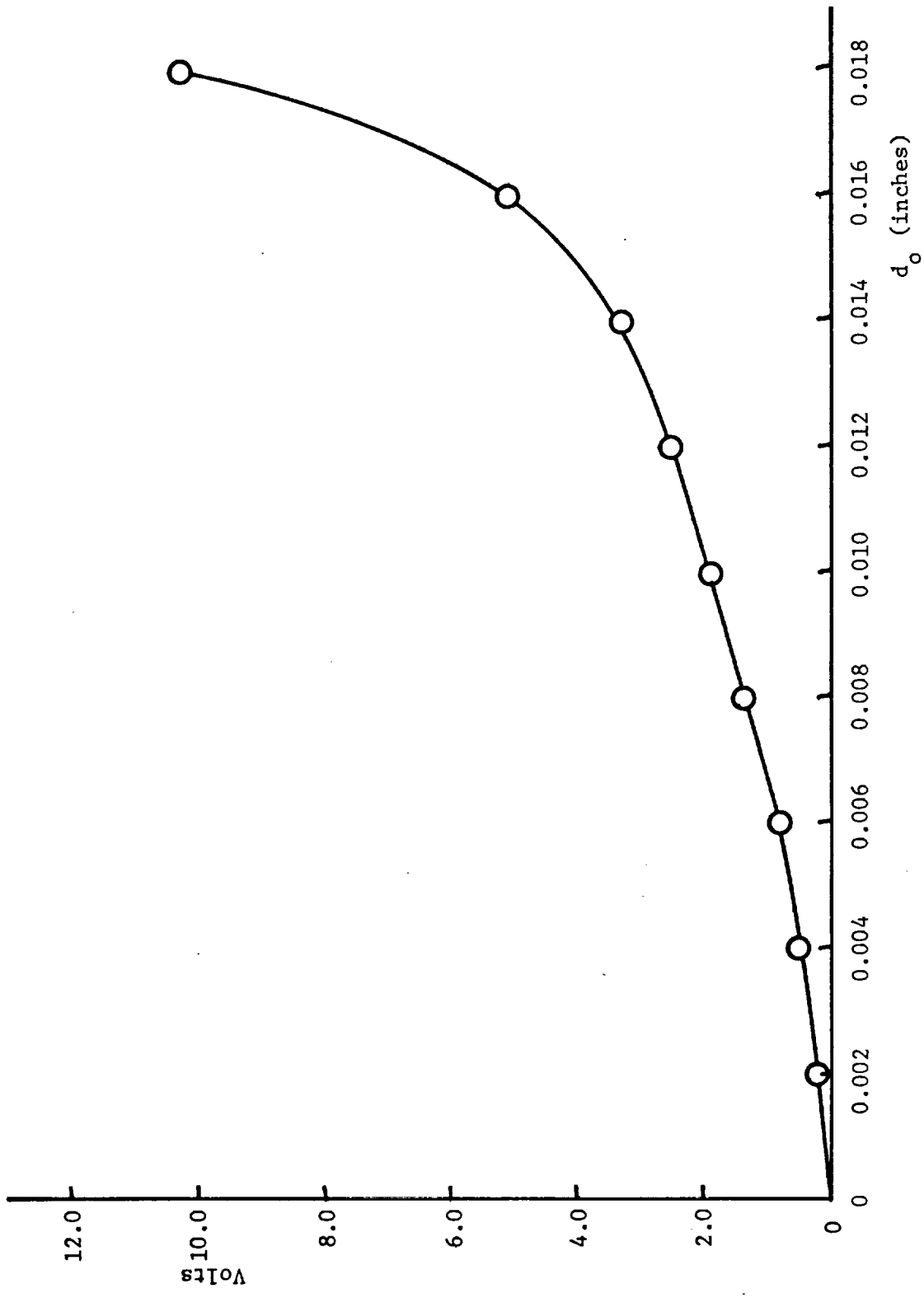

STATIC PICKUP CALIBRATION

Figure 28

APPENDIX A

Equipment Listing

1. Frequency Analyzer - Bruel & Kjaer, Type 2107

2. Loudspeaker - Electro-Voice, Wolverine LS15

3. Measuring Microscope - Gaertner Scientific, Catalog No. M103

4. Microphone - Bruel & Kjaer, Type 4136; with Type 2615 Cathode Follower, and Type UA 0035 Connector

5. Oscillator - Bruel & Kjaer, Type 1022

6. Oscillograph - Honeywell Visicorder, Model 1706

7. Oscilloscope - Tektronix, Type 502

8. Panel Motion Pickup - Bently Nevada, Model 302

9. Pistonphone - Bruel & Kjaer, Type 4220

10. Recorder - Bruel & Kjaer, Type 2305

APPENDIX B

Calibration Techniques

Aside from the calibration of the equipment used, which is described in the manuals for each piece of equipment, there are two basic calibrations to be made: calibration of the microphone system, and calibration of the plate-pickup system. See Appendix A, for all equipment mentioned.

Calibration of the microphone system is a relatively simple operation. The sound pressure level measured on the meter of the Frequency Analyzer is the simple addition of the indicated dB on the meter (dB_M), the setting of the meter dial (dB_{MR}), the setting of the range multiplier dial (dB_{RM}), and the "K" factor for the particular microphone-cartridge unit used. In the present case, the "K" factor was $K = + 35.9$ dB.

Since the present analysis makes use of a Graphic Level Recorder to record results, the technique for calibration is slightly different. Instead of using the meter reading of the Frequency Analyzer, the number of dB indicated by the stylus deflection of the recorder is used. Thus, the sound pressure level is the addition of the reading on the recorder (dB_R), the setting of the meter range dial (dB_{MR}), and the setting of the range multiplier dial (dB_{RM}).

To check this result, a Pistonphone was used. This device

puts out a constant tone of 124.0 dB at 250cps. Using the calibration technique outlined in the previous paragraphs, the sound level was found to be 2.4 dB high. Thus, for calibraiton of the microphone:

$$dB = dB_R + dB_{RM} + dB_{MR} - 2.4\ dB .$$

The calibration of the plate pickup system is more complicated, since the recorder is calibrated in dB, a logarithmic scale, and panel deflections are normally in inches, a linear scale. To alleviate this problem, a two part technique was used for calibration. First, the plate pickup was calibrated to an oscilloscope, taking advantage of the fact that the voltage reading of the oscilloscope is a linear scale, as are deflections. And then, the voltage reading of the oscilloscope was calibrated with the Graphic Level Recorder.

To calibrate the pickup with the oscilloscope, a static deflection technique was used. The pickup was set a distance, d_o, away from the panel using feeler gauges, and was connected to the oscilloscope to form a "base" reading. Then, the cavity was pressurized, allowing the panel to bulge outward a certain amount measured again by feeler gauges. This bulging of the panel caused a static deflection of the "base" reading on the oscilloscope. Thus, the difference between the two pickup measurements in inches could be compared to the voltage variation on the oscilloscope. This technique was used at various d_o

settings and for various panel static deflections. These deflection measurements were later checked optically, using a Measuring Microscope, thus verifying the data. Also, a dynamic check of panel deflections confirmed the authenticity of the static results. The use of a measuring microscope was tried to visually measure deflections; however, correlations between measurements obtained from a vibrating bar and measurements of the vibrating panel were poor.

Having obtained a plot of panel deflection versus oscilloscope voltage, the next step was to correlate panel deflection with the Graphic Level Recorder. The panel was excited with an external field of 100 dB at the panel center. From the previous calibration, a deflection of .0079" was noted on the oscilloscope. This deflection was then recorded so that the total dB (dB_T) recorded on the Graphic Level Recorder could be calibrated with panel deflections. This procedure was used for various pickup spacings, d_o, and panel deflections, δ. The calibration curves are shown in Figure 27, where

$$dB_T = dB_{MR} + dB_{RM} + dB_R .$$

To insure that the pickup was spaced exactly the same distance above the panel for each run, the measuring microscope was used to correlate pickup spacing, d_o, with static deflection on the oscilliscope. Thus, feeler gauges were not necessary to set pickup spacing. The calibration curve is shown in Figure 28.

APPENDIX C

Panel-Cavity Interaction Theory

The model to be considered, shown in Figure 1, is that of a rigid rectangular cavity with one flexible wall. Assume that the motions of the panel are sufficiently small so that the linearized form of the equations of motion may be employed. Needed will be three basic equations:

$$D\nabla^4 w + \beta \frac{\partial w}{\partial t} + m \frac{\partial^2 w}{\partial t^2} = (P_c - P_\infty^c) + \Delta P_{\text{external}} \tag{C-1}$$

$$\nabla^2 \phi_c - \frac{1}{a_c^2} \frac{\partial^2 \phi_c}{\partial t^2} = 0 \tag{C-2}$$

$$P_c - P_\infty^c = -\rho_c \frac{\partial \phi_c}{\partial t} \tag{C-3}$$

which are the plate equation of motion, the cavity equation of motion, and the pressure-velocity potential relation respectively, along with the boundary conditions for clamped edges:

(a) $\frac{\partial \phi_c}{\partial x} = 0 \qquad \text{on} \quad x = 0, a$

(b) $\frac{\partial \phi_c}{\partial y} = 0 \qquad \text{on} \quad y = 0, b$

(C-4)

(c) $\frac{\partial \phi_c}{\partial z} = 0 \qquad \text{on} \quad z = -d$

(d) $\frac{\partial \phi_c}{\partial z} = \frac{\partial w}{\partial t} \qquad \text{on} \quad z = 0$

Now, let

$$w = \sum_m \sum_n A_{mn}(t)\, \psi_m(x)\, \psi_n(y) \tag{C-5}$$

where

$$\psi_m(x) = \cos \frac{(m-1)\pi x}{a} - \cos \frac{(m+1)\pi x}{a}$$

$$\psi_n(y) = \cos \frac{(n-1)\pi y}{b} - \cos \frac{(n+1)\pi y}{b}$$

are appropriate to clamped edge boundary conditions.

Substituting (C-5) into (C-1), multiplying through by $\psi_r(x)\,\psi_s(y)$ and integrating over the plate area, (C-1), becomes (in non-dimensional terms)

$$\sum_m \sum_n \Big\{ \int \psi_m'''' \psi_r \, d\xi \int \psi_n \psi_s \, d\eta + 2(a/b)^2 \int \psi_m'' \psi_r \, d\xi \int \ddot{\psi}_n \psi_s \, d\eta + (a/b)^4 \int \psi_m \psi_r \, d\xi \int \ddot{\psi}_n \psi_s \, d\eta \Big\} + 2 \sum_m \sum_n \zeta K_{11} \frac{d}{d\tau}\left(\frac{A_{mn}}{h}\right) \int \psi_m \psi_r \, d\xi \int \psi_n \psi_s \, d\eta + \sum_m \sum_n \frac{d^2}{d\tau^2}\left(\frac{A_{mn}}{h}\right) \int \psi_m \psi_r \, d\xi \int \psi_n \psi_s \, d\eta = \lambda_c^* \sum_m \sum_n Q^c_{mrns} + Q^{external}_{rs} \tag{C-6}$$

where

$$Q^c_{mrns}(\tau) \equiv \frac{a}{h} \iint \frac{(P_c^{mn} - P_\infty^c)}{\rho_c a_c^2} \cdot \psi_r(\xi)\,\psi_s(\eta)\, d\xi\, d\eta \tag{C-7}$$

$$Q_{rs}^{external}(\tau) \equiv \int\int P_{external}\, \psi_r(\xi)\, \psi_s(\eta)\, d\xi\, d\eta \qquad (C\text{-}8)$$

Defining

$$C^1_{mr} \equiv \int \psi_m'''' \psi_r \, d\xi$$

$$C^2_{mr} \equiv \int \psi_m'' \psi_r \, d\xi$$

$$C^3_{mr} \equiv \int \psi_m \psi_r \, d\xi$$

then (C-6) may be rewritten as

$$\sum_m \sum_n a_{mn} \left\{ C^1_{mr} C^3_{ns} + 2(a/b)^2 C^2_{mr} C^2_{ns} + \left(\frac{a}{b}\right)^4 C^3_{mr} C^1_{ns} \right\} + 2 \sum_m \sum_n \beta K_{11} \frac{da_{mn}}{d\tau} C^3_{mr} C^3_{ns}$$

$$+ \sum_m \sum_n \frac{d^2 a_{mn}}{d\tau^2} C^3_{mr} C^3_{ns} = \lambda^*_c \sum_m \sum_n Q^c_{mrns} + Q^{external}_{rs} \qquad (C\text{-}9)$$

Now, note that $Q_{rs}^{external}$ may be determined from (C-8), given $P_{external}$, but the evaluation of Q^c_{mrns} will require more computation. Re-expanding the plate motion in terms of the

cavity modes, i.e.,

$$w = \sum_i \sum_j b_{ij} \cos \frac{i\pi x}{a} \cos \frac{j\pi y}{b} \tag{C-10}$$

and considering a single plate mode, i.e.,

$$w = A_{mn} \psi_m(\xi) \psi_n(\eta)$$

then we may obtain

$$b_{ij} = \frac{A_{mn} \int \psi_m(\xi) \cos i\pi\xi \, d\xi \int \psi_n(\eta) \cos j\pi\eta \, d\eta}{\int \cos^2 i\pi\xi \, d\xi \int \cos^2 j\pi\eta \, d\eta} \tag{C-11}$$

Expanding ϕ_c similarly

$$\phi_c = \sum_i \sum_j \Phi^c_{ij}(z,t) \cos \frac{i\pi x}{a} \cos \frac{j\pi y}{b} \tag{C-12}$$

Using (C-12), (C-2) becomes

$$\phi^c_{ij} \left[-\left(\frac{i\pi}{a}\right)^2 - \left(\frac{j\pi}{b}\right)^2 \right] + \frac{\partial^2 \phi^c_{ij}}{\partial z^2} - \frac{1}{a_c^2} \frac{\partial^2 \phi^c_{ij}}{\partial t^2} \tag{C-13}$$

and (C-4) becomes

$$\frac{\partial \phi^c_{ij}}{\partial z} = 0 \quad \text{on} \quad z = -d$$

$$\frac{\partial \phi^c_{ij}}{\partial z} = \frac{\partial b_{ij}}{\partial t} \quad \text{on} \quad z = 0$$

with (C-4), (a) and (b) identically satisfied by (C-12). Taking a Laplace transform with respect to time, (C-13) becomes

$$\frac{\partial^2 \Phi^c_{ij}}{\partial z^2} = k^2_{ij} \Phi^c_{ij} \tag{C-15}$$

where

$$k_{ij} \equiv \left[\frac{p^2}{a_c^2} + \left(\frac{i\pi}{a} \right)^2 + \left(\frac{j\pi}{b} \right)^2 \right]^{1/2} \tag{C-16}$$

and (C-14) becomes

$$\frac{\partial \Phi^c_{ij}}{\partial z} = 0 \quad \text{on} \quad z = -d$$

$$\frac{\partial \Phi^c_{ij}}{\partial z} = \frac{\partial B_{ij}}{\partial t} \quad \text{on} \quad z = 0 \tag{C-17}$$

The solution to (C-15) is

$$\Phi^c_{ij} = D^1_{ij} \sinh k_{ij} z + D^2_{ij} \cosh k_{ij} z$$

Using (C-17) to evaluate D^1_{ij} and D^2_{ij}

$$\Phi^c_{ij} = \frac{\partial B_{ij}}{\partial t} \left[\frac{\sinh k_{ij} z + \coth k_{ij} d \cosh k_{ij} z}{k_{ij}} \right] \tag{C-18}$$

and using (C-3)

$$(P_c - P^c_\infty)_{ij} = - \frac{\rho_c P}{k_{ij}} \frac{\partial B_{ij}}{\partial t} \left[\sinh k_{ij} z + \coth k_{ij} d \cosh k_{ij} z \right] \tag{C-19}$$

where

$$P_c - P_\infty^c = \sum_i \sum_j (P_c - P_\infty^c)_{ij} \cos \frac{i\pi x}{a} \cos \frac{j\pi y}{b} \qquad \text{(C-20)}$$

Inverting (C-19) and non-dimensionalizing

$$(P_c - P_\infty^c)_{ij} = - \frac{\rho_c a_c^2}{d} \int_0^{s_c} \frac{\partial b_{ij}}{\partial \sigma_c} K_{ij}(\zeta, s_c - \sigma_c)\, d\sigma_c \qquad \text{(C-21)}$$

where

$$K_{ij} = \frac{1}{2\pi i} \int_{-i\infty}^{+i\infty} \tilde{p} \left[\frac{\sinh \lambda_{ij} \zeta + \coth \lambda_{ij} \cosh \lambda_{ij} \zeta}{\lambda_{ij}} \right] \cdot e^{s_c \tilde{p} q_d}\, d\tilde{p} \qquad \text{(C-22)}$$

The evaluation of K_{ij} is considered by Dowell.[12] Finally, using (C-20) and (C-7)

$$Q^c_{mrns}(\tau) = \frac{a}{\pi} \sum_i \sum_j \left. \frac{(p_c - p^c_\infty)_{ij}}{\rho_c a_c^2} \right|_{z=0} \cdot \int_0^1 \cos i\pi\xi \, \psi_r(\xi)\, d\xi \int_0^1 \cos j\pi\eta \, \psi_s(\eta)\, d\eta . \tag{C-23}$$

Furthermore, using (C-11) and (C-21), (C-23) can be written

$$Q^c_{mrns}(\tau) = -\frac{a}{d} \sum_i \sum_j \frac{L_{mi} L_{nj} L_{ri} L_{sj}}{M_i M_j} \cdot \int_0^{S_c} \frac{\partial a_{mn}(\sigma_c)}{\partial \sigma_c} K_{ij}(\xi = 0;\, S_c - \sigma_c)\, d\sigma_c \tag{C-24}$$

where

$$L_{ri} \equiv \int_0^1 \psi_r(\xi) \cos i\pi\xi \, d\xi$$

$$M_i \equiv \int_0^1 \cos^2 i\pi\xi \, d\xi .$$

For shallow cavities, a/d >> 1, there is a simple approximation to (C-24) that is considered by Dowell.[12] It corresponds to

$$K_{oo} = 1$$

$$K_{ij} = 0 \qquad i = j \neq 0$$

Then (C-24) becomes

$$Q^c_{mrns} = -\frac{a}{d}\,\frac{L_{mo}L_{no}L_{ro}L_{so}}{M_o^2}\,a_{mn}(s_c) \tag{C-26}$$

Finally, consider the pressure distribution in the cavity. Using (C-11), (C-20), and (C-21) and summing over all plate modes

$$\frac{P_c - P^c_\infty}{\rho_c a_c^2 h/d} = \sum_m \sum_n \sum_i \sum_j \cos\frac{i\pi x}{a}\cos\frac{j\pi y}{b}\,\frac{L_{mi}L_{nj}}{M_i M_j} \cdot \int_0^{s_c} \frac{\partial a_{mn}(\sigma_c)}{\partial \sigma_c} K_{ij}(s; s_c - \sigma_c)\, d\sigma_c \tag{C-27}$$

Making the same approximation mentioned previously, (C-24) may

be written

$$\frac{P_c - P_\infty^c}{\rho_c a_c^2 h/d} = - \sum_m \sum_n \frac{L_{mo} L_{no}}{M_o^2} a_{mn}(s_c) \qquad \text{(C-28)}$$

The one mode approximation considered in this report is a simplification of the equations discussed in this appendix. It corresponds to $m = n = 1$, $r = s = 1$, $i = j = 0$. Then (C-9) becomes

$$a_{11} \left\{ C'_{11} C^3_{11} + 2 (a/b)^2 C^2_{11} C^2_{11} + (a/b)^4 C^3_{11} C'_{11} \right\}$$

$$+ 2 \beta K_{11} \frac{da_{11}}{d\tau} C^3_{11} C^3_{11} + \frac{d^2 a_{11}}{d\tau^2} C^3_{11} C^3_{11} = \qquad \text{(C-29)}$$

$$\lambda_c^* Q^c_{1111} + Q^{external}_{11}$$

where

$$Q^c_{1111} = - \frac{a}{d} \frac{L_{10}^4}{M_o^2} \int_0^{s_c} \frac{\partial a_{11}}{\partial \sigma_c} K_{oo}(\beta = 0; s_c - \sigma_c) \, d\sigma_c \qquad \text{(C-30)}$$

When a/d >> 1, the assumption can be made that

$$K_{oo} = 1$$

$$K_{ij} = 0 \qquad i = j \neq 0$$

then (C-29) becomes

$$a_{11}\left\{C_{11}^{1}C_{11}^{3} + 2(a/b)^{2}C_{11}^{2}C_{11}^{2} + (a/b)^{4}C_{11}^{3}C_{11}^{1}\right\}$$

$$+ 2\left\{K_{11}\frac{da_{11}}{d\tau}C_{11}^{3}C_{11}^{3} + \frac{d^{2}a_{11}}{d\tau^{2}}C_{11}^{3}C_{11}^{3} + \chi_{c}^{*}\frac{L_{10}^{4}}{M_{o}^{2}}\frac{a}{d}a_{11}\right. \tag{C-31}$$

$$= Q_{11}^{external}$$

Let

$$E_1 \equiv C_{11}^{1}C_{11}^{3} + 2(a/b)^{2}C_{11}^{2}C_{11}^{2} + (a/b)^{4}C_{11}^{3}C_{11}^{1}$$

$$+ \chi_{c}^{*}\frac{a}{d}\frac{L_{10}^{4}}{M_{o}^{4}}$$

$$E_2 \equiv C_{11}^{3}C_{11}^{3}$$

then (C-31) becomes

$$a_{11}E_1 + 2\zeta\Omega_{11}\frac{da_{11}}{d\tau}E_2 + \frac{d^{2}a_{11}}{d\tau^{2}}E_2 = Q_{11}^{random} \tag{C-32}$$

Assume

$$Q_{11}^{external} = \hat{Q}\, e^{i\Omega t} \tag{C-33}$$

then

$$a_{11} = \hat{a}_{11}\, e^{i\Omega t} \quad , \quad (P_c - P_\infty^c) = \widehat{(P_c - P_\infty^c)}\, e^{i\Omega t} \tag{C-34}$$

and

$$\hat{a}_{11}\left\{ E_1 + 2i\zeta\Omega_{11}\Omega E_2 - \Omega^2 E_2 \right\} = \hat{Q} \tag{C-35}$$

At resonance

$$\Omega^2 = \Omega_{11}^2 = E_1 / E_2$$

Thus, since

$$E_2 \hat{a}_{11}\left\{ \frac{E_1}{E_2} + 2i\zeta\Omega_{11}^2 - \Omega_{11}^2 \right\} = \hat{Q}$$

then

$$\hat{a}_{11}\left[2i\zeta\Omega_{11}^2 E_2 \right] = \hat{Q} \qquad \text{at resonance} \tag{C-36}$$

Finally, ratioing two amplitudes at two different cavity depths, (C-36) is used to develop the required result:

$$\frac{\hat{a}_{11}^{d_1}}{\hat{a}_{11}^{d_2}} = \left[\frac{\rho^{d_2}}{\rho^{d_1}}\right]\left[\frac{\Omega_{11}^{d_2}}{\Omega_{11}^{d_1}}\right]^2$$

Now, for cavity pressures, consider (C-27) with the assumptions of (C-33) and (C-34), and the assumption that a/d >> 1. Then (C-27) becomes

$$\frac{\widehat{(P_c - P_\infty^c)}}{\hat{a}_{11}} = -\frac{L_{10}^2}{M_0^2}\rho_c a_c^2 \frac{h}{d} \qquad \text{(C-37)}$$

Combining (C-36) and (C-37):

$$\frac{\widehat{(P_c - P_\infty^c)}}{\hat{Q}} = \frac{-\frac{L_{10}^2}{M_0^2}\rho_c a_c^2 h/d}{2i\rho\Omega_{11}^2 E_2} \qquad \text{(C-38)}$$

As before, ratioing two cavity pressures at two different cavity depths, (C-38) is used to develop the required result:

$$\frac{P^{d_1}}{P^{d_2}} = \left(\frac{d_2}{d_1}\right)\left[\frac{\rho^{d_2}}{\rho^{d_1}}\right]\left[\frac{\Omega^{d_2}}{\Omega^{d_1}}\right]^2$$

where $$\hat{P} \equiv \left(\widehat{P_c - P_\infty^c}\right) .$$